New Approximations and Tests of Linear Fluctuation-Response for Chaotic Nonlinear Forced-Dissipative Dynamical Systems

Rafail V. Abramov* Andrew J. Majda†

Abstract

We develop and test two novel computational approaches for predicting the mean linear response of a chaotic dynamical system to small change in external forcing via the fluctuation-dissipation theorem. Unlike the earlier work in developing fluctuation-dissipation theorem-type computational strategies for chaotic nonlinear systems with forcing and dissipation, the new methods are based on the theory of Sinai-Ruelle-Bowen probability measures, which commonly describe the equilibrium state of such dynamical systems. The new methods take into account the fact that the dynamics of chaotic nonlinear forced-dissipative systems often reside on chaotic fractal attractors, where the classical quasi-Gaussian formula of the fluctuation-dissipation theorem often fails to produce satisfactory response prediction, especially in dynamical regimes with weak and moderate degrees of chaos. A simple new low-dimensional chaotic nonlinear forced-dissipative model is used to study the response of both linear and nonlinear functions to small external forcing in a range of dynamical regimes with an adjustable degree of chaos. We demonstrate that the two new methods are remarkably superior to the classical fluctuation-dissipation formula with quasi-Gaussian approximation in weakly and moderately chaotic dynamical regimes, for both linear and nonlinear response functions. One straightforward algorithm gives excellent results for short-time response while the other algorithm, based on systematic rational approximation, improves the intermediate and long time response predictions.

1 Introduction

The fluctuation-dissipation theorem (FDT) is one of the cornerstones of modern statistical physics, discovered about eighty years ago. Roughly speaking, the fluctuation-dissipation theorem states that for dynamical systems at statistical equilibrium the average response to small external perturbations can be calculated through the knowledge of suitable correlation

*Department of Mathematics, Statistics and Computer Science, University of Illinois at Chicago

†Department of Mathematics and Center for Atmosphere Ocean Science, Courant Institute of Mathematical Sciences, New York University

functions of the unperturbed dynamical system. The fluctuation-dissipation theorem has great practical use in traditional setting involving statistical equilibrium of baths of identical gas or liquid molecules, Ornstein-Uhlenbeck Brownian motion, motion of electric charges, turbulence, quantum field theory, chemical physics, physical chemistry and other areas. The general advantage provided by the fluctuation-dissipation theorem is that one can successfully predict the response of a dynamical system at statistical equilibrium to an arbitrary small external perturbation without ever observing the behavior of the perturbed system, which offers great versatility and insight in understanding behavior of dynamical processes near equilibrium in numerous scientific applications [6, 12]. Typically, the linear response in the fluctuation-dissipation theorem is given as the time convolution of an external perturbation with the linear response operator in the form of specially crafted time correlation function, which is computed through the long-term observation of the unperturbed dynamical system at statistical equilibrium. The latter fact explains the interest towards the fluctuation-dissipation theorem among the computational community, because one can often compute a long-time trajectory of a dynamical system near statistical equilibrium through a direct numerical simulation, and calculate the linear response "on the fly" as numerical solution evolves by averaging its time series.

The fact that the fluctuation-dissipation theorem provides an approximation to the response of a dynamical system to a small change of its parameters by observing equilibrium statistical behavior of the unperturbed system makes it a convenient framework for studying long term global climate changes on the planetary scale. The response of climate dynamics on the planetary scale to changes of various global physical parameters is an area which is being extensively studied in contemporary atmosphere ocean science. The physical parameters controlling planetary climate dynamics range from solar radiation, to volcanic activity, greenhouse gas, ozone, polar ice melting and many others, which are normally computed via direct numerical simulation for an appropriate climate model. In the context of the fluctuation-dissipation theorem, one observes climatology of a model for sufficiently long time under the tacit assumption that the dynamics is close to its statistical equilibrium, and then applies the fluctuation-dissipation theorem to predict mean climate response to small changes of the physical parameters of the dynamics without actually simulating an appropriate scenario of climate development for those changes of parameters, which usually poses a computational problem of substantial complexity.

Despite the fact that the climate system is a complex chaotic multiscale problem with forcing, dissipation, and the equilibrium state structure has significant complexity, there has been a profound interest among the atmospheric/ocean science community to apply the fluctuation-dissipation theorem to predict global climate changes responding to variation of certain physical parameters. In the mid 1970s Leith [13] suggested the possibility that, despite the absence of the classical Gaussian equilibrium state, the fluctuation-dissipation theorem might constitute a sensible approximation for appropriate variables in the complex climate system. Leith's approximation has been called the quasi-Gaussian approximation in [16], where it is studied theoretically and computationally. Leith's suggestion has inspired others such as Bell [2], Carnevale et al. [3], and Dymnikov, Gritsoun and Branstator [7, 9, 10]

to apply the quasi-Gaussian fluctuation-dissipation theorem for idealized climate models with various approximations and numerical procedures. Bell [2] considered a special truncation of the barotropic vorticity equation and studied the response of this truncation to small kick of trajectory at initial time, reporting that the predictions of classical FDT for the response of the system hold extremely well. Carnevale et al. [3] generalize the Gaussian FDT formula to a non-Gaussian, although smooth, equilibrium state, also documenting reasonably high precision of the classical Gaussian FDT formula for one model [17], but also its poor approximation for the classical Lorenz 63 model. Dymnikov, Gritsoun and Branstator [7, 9, 10] developed a systematic procedure to compute the complete linear response operator in the matrix form for different response times, and also present a robust algorithm of verification for the FDT response prediction through a series of direct numerical simulations with the actual perturbed system. Gritsoun and Branstator [8] have applied the quasi-Gaussian approximation to a comprehensive general circulation model with interesting results. Craig and Cohen [4] applied the ideas of the classical FDT to the unresolved features of tropical convection and cloud formation.

The linear response of the forced-dissipative 40-mode Lorenz 96 model [1, 14, 15] within the framework of the quasi-Gaussian FDT has also been studied by the authors in [16]. It has been found in [16] that although the quasi-Gaussian FDT works reasonably well for the forced-dissipative Lorenz 96 model in strongly chaotic dynamical regimes, for weakly chaotic regimes the predictions of the classical FDT become much worse. While suitable for dynamical systems with a nearly canonical Gaussian equilibrium state, the fluctuation-dissipation theorem in its classical formulation is only partially successful for nonlinear dynamical systems with forcing and dissipation. The major difficulty in this situation is that the probability measure in the limit as time approaches infinity in this case is typically a Sinai-Ruelle-Bowen probability measure which is supported on a large-dimensional (often fractal) set and is usually not absolutely continuous with respect to the Lebesgue measure [5, 21]. In the context of Axiom A attractors, Ruelle [19, 20] has adapted the classical calculations for FDT to this setting.

Here in Section 2, using the recipes from [5, 19], we develop two practical numerical algorithms for computing linear response of a chaotic dynamical system to small external perturbation. These two methods have opposing strengths and weaknesses: the first method studied here applies for a largely arbitrary dynamical system, and is a perfect approach to evaluate linear response of an arbitrary system for short times but suffers from numerical instability for longer times; the second one is a rational approximation of Ruelle's FDT formula for an Axiom A attractor and is a better approximation for longer times in weakly and moderately chaotic dynamical regimes, where the quasi-Gaussian FDT approximation does not work well. Section 3 introduces a simple 5-mode nonlinear forced-dissipative model with remarkable mixing properties and an adjustable degree of chaos through a variable external forcing parameter. The model is based on the Lorenz 96 system [1, 14, 15]. In Section 4 we systematically compare and contrast the performance of the two new methods with the classical quasi-Gaussian FDT approach using this simple 5-mode model. It is demonstrated in Section 4 that the two new methods are remarkably superior to the classical quasi-Gaussian

FDT formula in weakly and moderately chaotic dynamical regimes for both linear and nonlinear observable response functions. The results of the current work are summarized in Section 5. Various practical computational strategies for the new FDT methods are detailed in Appendices A and B.

2 Linear Fluctuation-Dissipation and Systematic Approximations

Here we start with the fluctuation-dissipation theorem in its classical formulation for a dynamical system of chaotic ODEs for a vector $\vec{x} \in \mathbb{R}^N$, given by

$$\frac{\mathrm{d}\vec{x}}{\mathrm{d}t} = \vec{f}(\vec{x}), \tag{2.1}$$

where $\vec{f}$ is a vector field of dimension N. As discussed in [18], and also in Chapter 2 of [16], in the statistical dynamics of complex systems one is interested in the evolution of probability densities, $p(t, \vec{x})$, associated with (2.1) rather than individual solutions. It is well-known that the evolution of these probability densities, $p(t, \vec{x})$, satisfies the Liouville equation [18]

$$\begin{aligned} \frac{\partial}{\partial t} p(t, \vec{x}) &= L_L p(t, \vec{x}), \\ p(t, \vec{x})|_{t=0} &= p_0(\vec{x}), \end{aligned} \tag{2.2}$$

with $L_L p = -\operatorname{div}(\vec{f} p)$ being the Liouville operator.

The dynamical system in (2.1) is perturbed by small external forcing, $\delta\vec{f}(t, \vec{x})$, as

$$\frac{\mathrm{d}\vec{x}}{\mathrm{d}t} = \vec{f}(\vec{x}) + \delta\vec{f}(t, \vec{x}). \tag{2.3}$$

Then, similar to (2.2), the probability density $p^\delta(t, \vec{x})$ of the perturbed system in (2.3) satisfies an appropriately perturbed Liouville equation,

$$\begin{aligned} \frac{\partial}{\partial t} p^\delta(t, \vec{x}) &= L_L p^\delta(t, \vec{x}) + \delta L_L p^\delta(t, \vec{x}), \\ p^\delta(0, \vec{x}) &= p_0^\delta(\vec{x}), \end{aligned} \tag{2.4}$$

with $\delta L_L p = -\operatorname{div}(\delta\vec{f}(t, \vec{x}) p)$ being the part of the Liouville operator corresponding to small perturbation $\delta\vec{f}$ in (2.3). By $p_{eq}(\vec{x})$ we denote smooth rapidly decreasing (as $\|\vec{x}\| \to \infty$) equilibrium probability density for the unperturbed system in (2.2), so that

$$L_L p_{eq} = 0. \tag{2.5}$$

Further we assume a natural explicit time-space separable structure for the perturbation $\delta\vec{f}(t, \vec{x})$ in (2.3):

$$\delta\vec{f}(t, \vec{x}) = a(\vec{x})\delta\vec{f}(t), \tag{2.6}$$

with $a(\vec{x})$ being an $\vec{x}$-dependent matrix, and $\delta\vec{f}(t)$ being the time-dependent part of external forcing. Then, the Liouville operator δL_L in (2.4) can be written concisely as

$$\delta L_L p = \vec{L}_a p \cdot \delta\vec{f}(t) \tag{2.7}$$

with operator $\vec{L}_a$ given by

$$\vec{L}_a p = -\operatorname{div}(a(\vec{x})p). \tag{2.8}$$

In (2.8), the divergence of the matrix $a(\vec{x})p$ is a vector. In the case of space-independent external forcing $\delta\vec{f}(t,\vec{x}) = \delta\vec{f}(t)$ (so that $a(\vec{x})$ is the identity matrix) $\vec{L}_a$ assumes a simple form

$$\vec{L}_a p = -\nabla p. \tag{2.9}$$

Let $A(\vec{x})$ be a linear or nonlinear function whose mean response to small external forcing is to be predicted by the fluctuation-dissipation theorem. Here we assume that A is a scalar, however generalization to the vector-valued A is straightforward. The mean state, or expected value, of $A(\vec{x})$ with respect to the equilibrium probability density in (2.5) is, by definition, given by

$$E[A(\vec{x})] = \int_{\mathbb{R}^N} A(\vec{x}) p_{eq}(\vec{x}) \mathrm{d}\vec{x}. \tag{2.10}$$

The main statement of the fluctuation-dissipation theorem provides a formal procedure to calculate the change in expected value $\delta E[A(\vec{x})](t)$ for the perturbed system in (2.4) as

$$\delta E[A(\vec{x})](t) = \int_{\mathbb{R}^N} A(\vec{x}) \delta p(t,\vec{x}) \mathrm{d}\vec{x} = \int_0^t \vec{R}(t-t') \cdot \delta\vec{f}(t') \mathrm{d}t', \tag{2.11}$$

where the vector linear response operator is given by

$$\vec{R}(t) = \int_{\mathbb{R}^N} A(\vec{x}) \left(\exp[tL_L][\vec{L}_a p_{eq}] \right)(\vec{x}) \mathrm{d}\vec{x}. \tag{2.12}$$

Note that the formula (2.12) depends only on the equilibrium state density p_{eq}, which means that behavior of the perturbed system from (2.4) does not need to be observed to compute (2.12). Formal systematic derivation of (2.11) and (2.12) is given in [18], and also Chapter 2 of [16]). For the special case with constant external forcing $\delta\vec{f} = const$ the linear response formula is simplified to

$$\delta E[A(\vec{x})](t) = \vec{\mathcal{R}}(t) \cdot \delta\vec{f}, \qquad \vec{\mathcal{R}}(t) = \int_0^t \vec{R}(t') \mathrm{d}t', \tag{2.13}$$

where $\vec{R}(t)$ is taken from (2.12). The general formula in (2.12) serves as the starting point for further approximations under various assumptions, leading to different versions of the fluctuation-dissipation theorem.

2.1 Short-time FDT

A wide variety of practical geophysical models are complex nonlinear chaotic forced-dissipative dynamical systems, whose solutions live on strange attractors. The equilibrium states on such attractors do not even possess densities p_{eq} with respect to Lebesgue measure. Due to this fact, it is desirable to rework the classical FDT formula in (2.12) and (2.13) in such a way that an approximation to the density p_{eq} of the equilibrium probability measure is not required to compute the linear response. We develop such a method below, which we call short-time FDT (ST-FDT), due to its inherent numerical instability at longer times for chaotic dynamical systems.

First, we introduce the operators $L_L^\dagger$ and $\vec{L}_a^\dagger$

$$L_L^\dagger = \vec{f} \cdot \nabla, \qquad \vec{L}_a^\dagger = a^T(\vec{x})\nabla, \tag{2.14}$$

which are adjoint to L_L and $\vec{L}_a$ under standard inner product generated by the Lebesgue measure, respectively. Then, integrating (2.12) by parts yields

$$\vec{R}(t) = \int_{\mathbb{R}^N} \left(\vec{L}_a^\dagger \exp[tL_L^\dagger] A(\vec{x}) \right) p_{eq} \mathrm{d}\vec{x}. \tag{2.15}$$

Using the solution operator $\vec{x} = \vec{X}(t, \vec{x}_0)$ with an initial condition $\vec{x}_0$, we show that the action of $\exp[tL_L^\dagger]A$ is equivalent to the computation of $A(\vec{X}(t, \vec{x}))$. First we define $\mathcal{A} : [T \times \mathbb{R}^N] \to \mathbb{R}$ as

$$\mathcal{A}(t, \vec{x}) = A(\vec{X}(-t, \vec{x})) = A(\vec{x}_0) \tag{2.16}$$

using the fact that the system in (2.1) is autonomous (i.e. its right-hand side does not depend explicitly on time). Since, according to (2.16), the time derivative of $\mathcal{A}$ is zero, $\mathcal{A}(t, \vec{x})$ satisfies the following identity:

$$\frac{\partial \mathcal{A}}{\partial t} + L_L^\dagger \mathcal{A} = \frac{\mathrm{d}\mathcal{A}}{\mathrm{d}t} = 0. \tag{2.17}$$

On the other hand, formal solution to the partial differential equation in (2.17) is

$$\mathcal{A}(t, \vec{x}) = \exp[-tL_L^\dagger] \mathcal{A}(0, \vec{x}), \tag{2.18}$$

and thus, recalling that $\mathcal{A}(0, \vec{x}) = A(\vec{x})$ and replacing t with $-t$, we obtain

$$\exp[tL_L^\dagger] A(\vec{x}) = A(\vec{X}(t, \vec{x})). \tag{2.19}$$

The fluctuation-dissipation formula in (2.15) then becomes

$$\vec{R}(t) = \int_{\mathbb{R}^N} \left(\vec{L}_a^\dagger A(\vec{X}(t, \vec{x})) \right) p_{eq} \mathrm{d}\vec{x}. \tag{2.20}$$

Here and below in the remainder of the paper we assume ergodicity for (2.1), so that for almost every trajectory $\vec{x}(t)$,

$$\lim_{r \to \infty} \frac{1}{r} \int_0^r g(\vec{x}(t)) \mathrm{d}t = \int_{\mathbb{R}^N} g(\vec{x}) \mathrm{d}p_{eq}(\vec{x}). \tag{2.21}$$

Using (2.21) and replacing the phase space average $\mathrm{d}p_{eq}(\vec{x})$ with the time average for (2.20) and recalling the form of $\vec{L}_a^\dagger$ from (2.14) yields

$$\vec{R}(\tau) = \lim_{r\to\infty} \frac{1}{r} \int_0^r \nabla_{\vec{x}(t)} A\left(\vec{x}(t+\tau)\right) a(\vec{x}(t))\mathrm{d}t. \tag{2.22}$$

The nonlocal derivative $\nabla_{\vec{x}(t)} A\left(\vec{x}(t+\tau)\right)$ is computed via the tangent map (or, as it is sometimes called, the tangent propagator)

$$T^\tau_{\vec{x}(t)} = \exp\left(\int_t^{t+\tau} \nabla \vec{f}(\vec{x}(s))\mathrm{d}s\right) \tag{2.23}$$

as

$$\vec{R}_{ST-FDT}(\tau) = \lim_{r\to\infty} \frac{1}{r} \int_0^r \nabla A\left(\vec{x}(t+\tau)\right) T^\tau_{\vec{x}(t)} a(\vec{x}(t))\mathrm{d}t, \tag{2.24}$$

while the tangent map itself is obtained by solving the equation

$$\frac{\mathrm{d}T^\tau_{\vec{x}(t)}}{\mathrm{d}\tau} = \nabla \vec{f}(\vec{x}(t+\tau)) T^\tau_{\vec{x}(t)}. \tag{2.25}$$

A practical algorithm to compute the solution of (2.25) is given in the Appendix A. For constant external forcing δf, the formula (2.13) is written here as

$$\begin{aligned} \delta E[A(\vec{x})]_{ST-FDT}(t) &= \vec{\mathcal{R}}_{ST-FDT}(t) \cdot \delta \vec{f}, \\ \vec{\mathcal{R}}_{ST-FDT}(s) &= \lim_{r\to\infty} \frac{1}{r} \int_0^r \mathrm{d}t \int_0^s \nabla A\left(\vec{x}(t+\tau)\right) T^\tau_{\vec{x}(t)} \mathrm{d}\tau. \end{aligned} \tag{2.26}$$

Note that the linear response formulas in (2.24) and (2.26) do not include the equilibrium probability density p_{eq}. The latter property makes them suitable for computing the linear response for an arbitrary equilibrium state, even if it does not possess probability density with respect to the Lebesgue measure. The main drawback of (2.24) and (2.26) is that the tangent map in (2.23) undergoes exponential blow-up in time due to the presence of positive Lyapunov characteristic exponents in chaotic dynamical systems, and thus (2.24) and (2.26) can only be used for limited time intervals.

2.2 Classical formula for FDT

Following the derivation in [18] or Chapter 2 of [16], the classical FDT formula for the linear response vector $\vec{R}(t)$ in (2.12) is expressed as the time autocorrelation function

$$\vec{R}(\tau) = \langle A(\vec{x}(t+\tau)) \vec{B}(\vec{x}(t)) \rangle, \tag{2.27}$$

where the long-term trajectory $\vec{x}(t)$ is observed for the unperturbed system, with the special function $\vec{B}(\vec{x})$,

$$\vec{B}(\vec{x}) = \frac{\vec{L}_a(\vec{x}) p_{eq}(\vec{x})}{p_{eq}(\vec{x})}, \tag{2.28}$$

where the correlation vector on the right hand size of (2.27) is evaluated at the unperturbed state. Replacing phase space average with time average in (2.27) yields

$$\vec{R}(\tau) = \lim_{T\to\infty} \frac{1}{T} \int_0^T A(\vec{x}(t+\tau)) \frac{\vec{L}_a p_{eq}(\vec{x}(t))}{p_{eq}(\vec{x}(t))} \mathrm{d}t. \tag{2.29}$$

For constant external forcing δf, the formula (2.13) is written here as

$$\begin{gathered} \delta E[A(\vec{x})](t) = \vec{\mathcal{R}}(t) \cdot \delta \vec{f}, \\ \vec{\mathcal{R}}(s) = -\lim_{T\to\infty} \frac{1}{T} \int_0^T \mathrm{d}t \int_0^s A(\vec{x}(t+\tau)) \frac{\nabla p_{eq}(\vec{x}(t))}{p_{eq}(\vec{x}(t))} \mathrm{d}\tau, \end{gathered} \tag{2.30}$$

where we take into account the form of $\vec{L}_a$ in (2.9) for constant external forcing. Note that the correlation function can be evaluated from historical observations without explicit knowledge of the right hand side of the unperturbed system in (2.1). However, knowledge of the equilibrium probability density p_{eq} or its approximation is required for computing (2.29). Also note that for equilibrium states which are not absolutely continuous with respect to the Lebesgue measure (i.e. do not possess density p_{eq}) the classical formulas in (2.29) and (2.30) formally become meaningless. However, as noted in [16], if suitable random noise is added to (2.1), p_{eq} becomes smooth and unique so the above formal manipulations are readily justified. On the other hand, even without noise, many interesting nonlinear systems have Gaussian invariant measures and the above formulation leads to exact predictions of linear response. These predictions have been tested in Chapter 2 of [16] for three diverse dynamical systems with Gaussian invariant measures and forty degrees of freedom with excellent agreement.

2.3 Quasi-Gaussian FDT

The quasi-Gaussian FDT (further qG-FDT) approximation is obtained from (2.27) and (2.28) by replacing the equilibrium probability density p_{eq} with its Gaussian approximation p_G

$$p_G(\vec{x}) = \frac{1}{(2\pi \det \sigma^2)^{N/2}} \exp\left(-\frac{1}{2} (\vec{x} - \bar{\vec{x}}) \sigma^{-2} (\vec{x} - \bar{\vec{x}}) \right), \tag{2.31}$$

with the mean state $\bar{\vec{x}}$ and covariance matrix σ^2 matching those of p_{eq}. Additionally, here it is assumed that the external forcing $\delta \vec{f}$ is $\vec{x}$-independent such that $\vec{L}_a$ has the simplified form in (2.9). Under these assumptions, the function $B(\vec{x})$ from (2.28) becomes

$$B_G(\vec{x}) = \sigma^{-2}(\vec{x} - \bar{\vec{x}}), \tag{2.32}$$

and the formula for the kernel $\vec{R}(\tau)$ of the linear response operator in (2.29) turns out to be a simple time autocorrelation function

$$\vec{R}_{qG-FDT}(\tau) = \lim_{r\to\infty} \frac{1}{r} \int_0^r A(\vec{x}(t+\tau)) \sigma^{-2} (\vec{x}(t) - \bar{\vec{x}}) \mathrm{d}t. \tag{2.33}$$

For constant external forcing $\delta\vec{f}$, the formula (2.13) is written here as

$$\begin{aligned} \delta E[A(\vec{x})]_{qG-FDT}(t) &= \vec{\mathcal{R}}_{qG-FDT}(t)\cdot\delta\vec{f}, \\ \vec{\mathcal{R}}_{qG-FDT}(s) &= \lim_{r\to\infty}\frac{1}{r}\int_0^r \mathrm{d}t\int_0^s A(\vec{x}(t+\tau))\sigma^{-2}(\vec{x}(t)-\bar{\vec{x}})\mathrm{d}\tau. \end{aligned} \tag{2.34}$$

The prefix "quasi" in the name of the quasi-Gaussian FDT formula comes from the fact that although the equilibrium density p_{eq} in the linear response operator is simplified by the Gaussian approximation, the time averaging process in (2.33) corresponds to the phase space averaging with respect to the true equilibrium state, rather than its Gaussian approximation. For details, see Chapter 2 of [16]. This is the form of FDT advocated by Leith [13] in his seminal paper. Section 2.7 of [16] contains a rigorous analysis of the validity of this approximation for short times.

2.4 Axiom A FDT

The main drawback of the ST-FDT formula in (2.24) is that it can only be used for limited time intervals of τ, due to the fact that the tangent map $T^\tau_{\vec{x}}$ undergoes exponential blow-up in the directions associated with positive Lyapunov characteristic exponents. Here, under the assumption of an Axiom A flow $\vec{X}(t,\vec{x})$ which settles onto a strange attractor $\mathcal{K}$, we avoid numerical instability in the short-time FDT approach in (2.24) by following the directions given in [20].

With help of Axiom A, one can uniformly decompose the small perturbation $\delta\vec{f}(t,\vec{x})$ into the sum of three components at each point of the trajectory $x(t)$ on the attractor:

$$\delta\vec{f}(t,\vec{x}) = P^+_{\vec{x}}\delta\vec{f}(t,\vec{x}) + P^-_{\vec{x}}\delta\vec{f}(t,\vec{x}) + P^0_{\vec{x}}\delta\vec{f}(t,\vec{x}), \tag{2.35}$$

where $P^+_{\vec{x}}$, $P^-_{\vec{x}}$ and $P^0_{\vec{x}}$ are the projection operators onto the expanding subspace $E^+_{\vec{x}}$, contracting subspace $E^-_{\vec{x}}$ and neutrally stable subspace E^0, consisting of only one vector $\vec{f}(\vec{x})$ (which is tangent to the direction of trajectory $\vec{x}(t)$), of the tangent bundle $T\mathcal{K}$ over the strange attractor $\mathcal{K}$ at $\vec{x}$. From a practical standpoint, $P^+_{\vec{x}}$ projects onto the span of the eigenvectors for positive Lyapunov exponents at $\vec{x}$, and $P^-_{\vec{x}}$ projects onto the span of the eigenvectors for negative Lyapunov exponents at $\vec{x}$. The neutral direction corresponds to zero Lyapunov exponent. For rigorous definition and detailed description of $E^+_{\vec{x}}$ and $E^-_{\vec{x}}$ see [5]. The formula for the Lyapunov characteristic exponents and their eigenvectors is also given below in Section 3, equation (3.4). All projection operators in (2.35) are computed from the tangent map $T^\tau_{\vec{x}}$ (see Appendix B for numerical algorithm).

With (2.35), (2.24) becomes

$$\vec{R}_{A-FDT}(\tau) = \vec{R}^{+}(\tau) + \vec{R}^{0-}(\tau), \tag{2.36}$$

with the corresponding expanding and neutral-contracting response operators

$$\vec{R}^{+}(\tau) = \lim_{r\to\infty}\frac{1}{r}\int_0^r \nabla A(\vec{x}(t+\tau))T^\tau_{\vec{x}(t)}P^+_{\vec{x}(t)}a(\vec{x}(t))\mathrm{d}t, \tag{2.37a}$$

$$\vec{R}^{0-}(\tau) = \lim_{r\to\infty} \frac{1}{r} \int_0^r \nabla A(\vec{x}(t+\tau)) T^{\tau}_{\vec{x}(t)} (P^0_{\vec{x}(t)} + P^-_{\vec{x}(t)}) a(\vec{x}(t)) \mathrm{d}t. \tag{2.37b}$$

The reason why the neutral and contracting operators P^0 and P^- are bundled together in (2.37) is that when the model is time-discretized for numerical computation, a stable time integrator is needed, which is a slightly contracting map from one discretization point to another to ensure numerical stability; this results in P^0 being rather slightly contracting rather than neutral (this is also the reason why the zero Lyapunov exponent is normally slightly below zero in stable numerical simulations). At this point, the exploding part of $\vec{R}(\tau)$ due to positive Lyapunov exponents is isolated in $\vec{R}^+(\tau)$, while computation of $\vec{R}^{0-}(\tau)$ becomes numerically stable. For the response on the expanding directions of the attractor, we follow [20] which utilizes the relative smoothness of the attractor in the expanding directions. For $\vec{R}^+(\tau)$, we use the statement b of Theorem 3.1 from [19] and "integrate by parts" in the formula for $R^+(\tau)$ in (2.37a); replacing the spatial average by the time average, we obtain

$$\vec{R}^+(\tau) = \lim_{r\to\infty} \frac{1}{r} \int_0^r A(\vec{x}(t+\tau)) \, \mathrm{div}^+ \left(P^+_{\vec{x}(t)} a(\vec{x}(t)) \right) \mathrm{d}t, \tag{2.38}$$

where div^+ denotes the divergence operator in the expanding subspace E^+. As one can observe, the tangent map $T^{\tau}_{\vec{x}(t)}$ is now absent from the formula (2.38) for the expanding linear response operator $\vec{R}^+(\tau)$, thus neutralizing its numerical instability. As noted already in [20], the formula for $\vec{R}^+(\tau)$ in (2.37a) is the direct analog of the classical FDT for smooth equilibrium measures from (2.29); on the other hand, the formula for $\vec{R}^{0-}(\tau)$ in (2.37b) the generally fractal dissipative directions of the attractor and has no direct analogue in the classical FDT.

Although lacking exponential numerical blow-up in time, the Axiom A FDT formula in (2.38) contains $\mathrm{div}^+ P^+$, which requires knowledge of spatial derivatives of the tangent map $T^{\tau}_{\vec{x}}$. Despite the fact that the equation which describes time evolution of $\partial_{\vec{x}} T^{\tau}_{\vec{x}}$ can be readily written, no reliable numerically stable method has been developed yet to compute $\partial_{\vec{x}} T^{\tau}_{\vec{x}}$ in practice. Instead, below we suggest a hybrid approximation to (2.38), based on the fact that SRB measures are relatively smooth in $E^+_{\vec{x}}$.

2.5 Hybrid Axiom A FDT

Here we develop a rational approximation to the expanding response operator, $\vec{R}^+(\tau)$ in the Axiom A FDT formula in (2.38). One reason for this is the numerical difficulty noted above in reliably calculating the unstable divergence. A second, more fundamental reason is that it is doubtful that most realistic physical systems have Axiom A attractors anyway, so an exact solution formula for A-FDT would still involve an approximation, and, therefore, a different rational approximation might be appropriate. To develop the new approximation, we first remark that (2.38) represents $\vec{R}^+(\tau)$ as a time correlation function

$$\vec{R}^+(\tau) = \langle A(\vec{x}(t+\tau)) \vec{B}^+(\vec{x}(t)) \rangle \tag{2.39}$$

with

$$\vec{B}^+(\vec{x}) = \operatorname{div}^+(P^+ a(\vec{x})). \tag{2.40}$$

Our idea is to utilize the quasi-Gaussian approximation projected on the expanding directions of the attractor where the invariant measure is absolutely continuous with respect to Lebesgue measure; thus, following (2.31) and (2.32) with special constant external forcing, we replace $\vec{B}^+(\vec{x})$ in (2.38) by $\vec{B}^+_G(\vec{x})$ given by

$$\vec{B}^+_G(\vec{x}) = P^+_{\vec{x}} \sigma^{-2}(\vec{x} - \bar{\vec{x}}). \tag{2.41}$$

The result is the hybrid A-FDT (hA-FDT) approximation

$$\vec{R}^+_{hA-FDT}(\tau) = \lim_{r\to\infty} \frac{1}{r} \int_0^r A(\vec{x}(t+\tau)) P^+_{\vec{x}(t)} \sigma^{-2}(\vec{x}(t) - \bar{\vec{x}}) \mathrm{d}t. \tag{2.42}$$

If this formula is combined with the formula in (2.37b) for $\vec{R}^{0-}(\tau)$ involving the response for the contracting directions, for constant external forcing we obtain the hybrid A-FDT approximation:

$$\begin{aligned}
\delta E[A(\vec{x})]_{hA-FDT}(t) &= \vec{\mathcal{R}}_{hA-FDT}(t) \cdot \delta\vec{f}, \\
\vec{\mathcal{R}}_{hA-FDT}(t) &= \vec{\mathcal{R}}^+_{hA-FDT}(t) + \vec{\mathcal{R}}^{0-}_{hA-FDT}(t), \\
\vec{\mathcal{R}}^+_{hA-FDT}(s) &= \lim_{r\to\infty} \frac{1}{r} \int_0^r \mathrm{d}t \int_0^s A(\vec{x}(t+\tau)) P^+_{\vec{x}(t)} \sigma^{-2}(\vec{x}(t) - \bar{\vec{x}}) \mathrm{d}\tau, \\
\vec{\mathcal{R}}^{0-}_{hA-FDT}(s) &= \lim_{r\to\infty} \frac{1}{r} \int_0^r \mathrm{d}t \int_0^s \nabla A(\vec{x}(t+\tau)) T^\tau_{\vec{x}(t)} (P^0_{\vec{x}(t)} + P^-_{\vec{x}(t)}) \mathrm{d}\tau.
\end{aligned} \tag{2.43}$$

The hybrid Axiom A FDT is a compromise between the ST-FDT and qG-FDT, inheriting essential features of both.

3 Two low-dimensional nonlinear forced-dissipative models with adjustable chaotic behavior

To study the new FDT approximations, developed in Section 2, one has to choose a test model of the form (2.1) which is nonlinear, forced-dissipative, has complex chaotic behavior, and is at the same time relatively simple and low-dimensional for easy practical implementation and robust numerical computations. Here we look at the Orszag-McLaughlin family of models [17] of the form

$$\frac{\mathrm{d}x_j}{\mathrm{d}t} = a x_{j+1} x_{j+2} + b x_{j-1} x_{j-2} + c x_{j+1} x_{j-1} - x_j + F \tag{3.1}$$

with periodic boundary conditions, and additional constant forcing F with linear dissipation $-x_j$ which are not present in the original model in [17]. Here a, b, c are constant coefficients,

satisfying the relation $a + b + c = 1$ in order to conserve energy without dissipation and forcing. It is interesting that the model in (3.1) with the coefficients a, b, c set to $0, -1, 1$, respectively, is independently introduced in [14, 15] as a simple nonlinear chaotic dynamical system with features which mimic certain large scale mechanisms of planetary dynamics such as Rossby waves. This Lorenz 96 (L96) model has been used by the present authors for studies of predictability [1, 11] and the fluctuation-dissipation theorem in the classical setting [16].

To provide a robust test for FDT approximations, we want a low-dimensional version of (3.1) which is strongly mixing yet has diverse behavior as F is varied. Here we study statistical behavior of the Orszag-McLaughlin model in (3.1) in two configurations to contrast their chaotic features.

1. **5-mode Lorenz 96 (L96) model:** The dimension of the model is set to $N = 5$, and the coefficients a, b, c of (3.1) are set to $0, -1, 1$, respectively. The model equation thus is
$$\frac{\mathrm{d}x_j}{\mathrm{d}t} = (x_{j+1} - x_{j-2})x_{j-1} - x_j + F, \tag{3.2}$$
where the value of F determines the dynamical for the L96 model: for lower values of F (3.2) exhibits weakly chaotic and quasiperiodic behavior, whereas for larger values of F the Lorenz 96 model in (3.2) behaves strongly chaotically. It is demonstrated in [16] that in the limit as $F \to \infty$, the L96 model in appropriately rescaled variables loses the forcing and dissipation terms, possesses the Liouville property and conserves quadratic energy [1].

2. **5-mode Anti Lorenz 96 (AL96) model:** The dimension of the model is again set to $N = 5$, and the coefficients a, b, c of (3.1) have reverse signs (hence it is dubbed AL96), i.e. $0, 1, -1$, respectively, such that the nonlinear part of L96 assumes opposite sign. The model equation thus is
$$\frac{\mathrm{d}x_j}{\mathrm{d}t} = (x_{j-2} - x_{j+1})x_{j-1} - x_j + F. \tag{3.3}$$
Just as for L96 in (3.2), the value of F can be adjusted to achieve various dynamical regimes for the AL96 model, with larger values of F corresponding to more chaotic dynamical regimes.

The dimension of the phase space is set to $N = 5$ for both models. Such a low-dimensional set-up significantly simplifies computation of time correlation functions for matrices such as the tangent map $T^t_{\vec{x}}$, which in this case has $5 \times 5 = 25$ entries (see Appendix A for details).

Before testing various fluctuation-response approaches of Section 2 on the models suggested above, one has to choose suitable dynamical regimes with sufficiently robust mixing properties. This is required by the fact that each linear response operator $\vec{R}(\tau)$ is essentially a time autocorrelation function, which has to be computed over a single long time trajectory $\vec{x}(t)$. Thus, if the dynamical regime is weakly mixing, the precise computation of linear response operators is difficult due to the fact that it has to be done over an extremely long

time trajectory to compensate for the lack of mixing and achieve a good time average. On the other hand, a variable degree of chaos is desired for testing the new FDT approaches in both strongly chaotic and weakly chaotic (but mixing!) regimes to systematically compare and contrast the advantages and drawbacks of the classical Gaussian FDT and new FDT approaches for each regime. In this section we select a set of suitable mixing dynamical regimes with a wide range of chaos by studying various aspects of statistical behavior of both models. The complete list of numerical techniques and parameters for both models is the following:

- Number of degrees of freedom $N = 5$;
- 4th-order Runge-Kutta time integrator;
- Numerical time step $\Delta t = 1/64$;
- Values of constant forcing $F = 6, 8, 12, 16$;
- Averaging time window for computing long-term time averages is $T = 500000$ time units;
- Initial spin-up time $T_0 = 10000$ is skipped before computing averages to let the numerical trajectory land on the attractor.

Below we present the results of numerical study of long-term statistical properties for both L96 and AL96 models.

3.1 Lyapunov characteristic exponents

The Lyapunov characteristic exponents are defined as follows: let

$$\Lambda_{\vec{x}} = \lim_{t\to\infty} \frac{1}{2t} \ln\left(T_{\vec{x}}^{tT} T_{\vec{x}}^{t}\right), \tag{3.4}$$

where $T_{\vec{x}}^t$ is the tangent map at $\vec{x}$ to $\vec{X}(t, \vec{x})$, defined in (2.23). Then the eigenvalues of $\Lambda_{\vec{x}}$, arranged in descending order $\lambda_1 \geq \lambda_2 \geq \ldots \geq \lambda_N$, are called the Lyapunov characteristic exponents. According to the Oseledec's multiplicative ergodic theorem (see [5] for details), for a given dynamical system the Lyapunov exponents are constants regardless of $\vec{x}$ almost everywhere, provided that the invariant SRB measure associated with the dynamical system is irreducible on the strange attractor $\mathcal{K}$, which is our tacit assumption.

The values of Lyapunov exponents have the following physical meaning: let $E_{\vec{x}}^i$ denote the subspace at $\vec{x}$ spanned by eigenvectors of $\Lambda_{\vec{x}}$, associated with the Lyapunov exponents $\lambda_i, \lambda_{i+1}, \ldots, \lambda_N$. By construction, these subspaces are nested: $E_{\vec{x}}^1 \supset E_{\vec{x}}^2 \supset \ldots \supset E_{\vec{x}}^N$. Note that, contrary to the Lyapunov exponents, the characteristic subspaces $E_{\vec{x}}^1, \ldots, E_{\vec{x}}^N$ actually depend on the point x. Then for any vector $\vec{u} \in E_{\vec{x}}^i \backslash E_{\vec{x}}^{i+1}$, its growth (or decay, depending on the sign of λ_i) under the action of the tangent map $T_{\vec{x}}^t$ can be estimated as

$$\|T_{\vec{x}}^t \vec{u}\| \sim e^{\lambda_i t}. \tag{3.5}$$

L96, $F = 6$	
$\lambda_1 = 0.8239$	$\lambda_2 = 0.2242$
$\lambda_3 = -0.7791$	$\lambda_4 = -1.514$
$\lambda_5 = -3.754$	

AL96, $F = 6$	
$\lambda_1 = 0.8185$	$\lambda_2 = 1.866 \cdot 10^{-2}$
$\lambda_3 = -0.5141$	$\lambda_4 = -1.44$
$\lambda_5 = -3.884$	

L96, $F = 8$	
$\lambda_1 = 1.452$	$\lambda_2 = 0.3188$
$\lambda_3 = -0.8825$	$\lambda_4 = -1.812$
$\lambda_5 = -4.076$	

AL96, $F = 8$	
$\lambda_1 = 1.447$	$\lambda_2 = 0.2758$
$\lambda_3 = -0.4887$	$\lambda_4 = -1.862$
$\lambda_5 = -4.372$	

L96, $F = 12$	
$\lambda_1 = 2.402$	$\lambda_2 = 0.7796$
$\lambda_3 = -0.7657$	$\lambda_4 = -2.199$
$\lambda_5 = -5.218$	

AL96, $F = 12$	
$\lambda_1 = 2.37$	$\lambda_2 = 0.7695$
$\lambda_3 = -0.4677$	$\lambda_4 = -2.416$
$\lambda_5 = -5.256$	

L96, $F = 16$	
$\lambda_1 = 3.174$	$\lambda_2 = 1.093$
$\lambda_3 = -0.8012$	$\lambda_4 = -2.541$
$\lambda_5 = -5.931$	

AL96, $F = 16$	
$\lambda_1 = 2.992$	$\lambda_2 = 1.127$
$\lambda_3 = -0.4074$	$\lambda_4 = -2.737$
$\lambda_5 = -5.976$	

Table 3.1: The Lyapunov exponents for the 5-mode L96 and AL96 models in the dynamical regimes with constant forcing F set to $6, 8, 12$ and 16.

Due to the estimate in (3.5) and their invariance over the attractor $\mathcal{K}$, the Lyapunov characteristic exponents are conventionally regarded as a natural measure of chaos in a dynamical system.

The Lyapunov characteristic exponents for the 5-dimensional L96 and AL96 models in the dynamical regimes of $F = 6, 8, 12, 16$ are displayed in Table 3.1. One can observe that in each case both models possess two positive Lyapunov exponents, which means that the corresponding dynamical regimes are chaotic. The positive Lyapunov exponents also grow as the forcing parameter F is increased, thus confirming that both L96 and AL96 models become more chaotic with stronger forcing. It can also be noticed that the L96 model appears to be slightly more chaotic with this measure than the AL96 model for the same values of forcing.

3.2 Moments and probability density functions

In this section we display the long-time averaged mean state, variance, skewness (3rd moment) and flatness (4th moment) of both the L96 and AL96 models, as well as the probability density functions (PDF) of phase space coordinates for both L96 and AL96 models. Here, since invariant probability measures on strange attractors do not possess densities

	Mean	Var	Skew	Flat
L96, $F = 6$	1.912	7.816	0.1095	2.042
AL96, $F = 6$	1.626	7.112	$-2.773 \cdot 10^{-2}$	2.368
L96, $F = 8$	2.302	13.12	0.1039	2.235
AL96, $F = 8$	1.914	11.65	$-4.305 \cdot 10^{-2}$	2.598
L96, $F = 12$	2.934	26.6	$5.962 \cdot 10^{-2}$	2.424
AL96, $F = 12$	2.312	22.4	-0.1216	2.706
L96, $F = 16$	3.258	41.52	$2.906 \cdot 10^{-2}$	2.491
AL96, $F = 16$	2.497	33.71	-0.1111	2.728

Table 3.2: The long-time mean state, variance, skewness and flatness for the 5-dimensional L96 and AL96 models with $F = 6, 8, 12$ and 16.

with respect to Lebesgue measure, the term "probability density function" should rather be understood in the sense of a long time histogram of the phase-space trajectory. While not being a true density, such a histogram still helps to understand how a long-time trajectory is distributed in the phase space. Quite often, the marginal densities of a strange attractor can be much smoother and this is happening empirically below.

The long-term averaged mean state $\bar{x}$ and moments M_p of the L96 and AL96 models are defined as

$$\begin{aligned} \bar{x} &= \lim_{T\to\infty} \frac{1}{T} \int_{T_0}^{T_0+T} x(t)\mathrm{d}t, \\ M_p &= \lim_{T\to\infty} \frac{1}{T} \int_{T_0}^{T_0+T} (x(t) - \bar{x})^p \, \mathrm{d}t, \end{aligned} \tag{3.6}$$

where, since both L96 and AL96 models are translationally invariant, any of the phase space coordinates $x_i(t)$, $1 \le i \le N$ (where in our case $N = 5$), can be taken as $x(t)$. Conventionally, the second moment M_2 is called variance, and the following nondimensional ratios $M_3/M_2^{3/2}$ and M_4/M_2^2 are called skewness and flatness, respectively. As mentioned above, the initial spin-up time $T_0 = 10000$ time units, and the long-term time averaging window $T = 500000$ time units.

The moments for both the L96 and AL96 models in the dynamical regimes with $F = 6, 8, 12, 16$ are displayed in Table 3.2. Observe that both the mean state and variance tend to grow with increasing forcing F. This is expected, since the coefficient for the linear dissipation term $-x_i$, which balances the forcing F, stays constant. Also, as F increases, the magnitude of the 3rd moment (skewness) for the L96 model tends to decrease, while for AL96 model it tends to increase. As for the 4th moment (flatness), it increases with increasing F, but does not reach the Gaussian value of 3.

Due to translational invariance of both the L96 and AL96 models, all phase space variables share a common long time probability density function. The PDFs for the physical space variables, computed via the standard bin-counting procedure [16], are shown in Figures

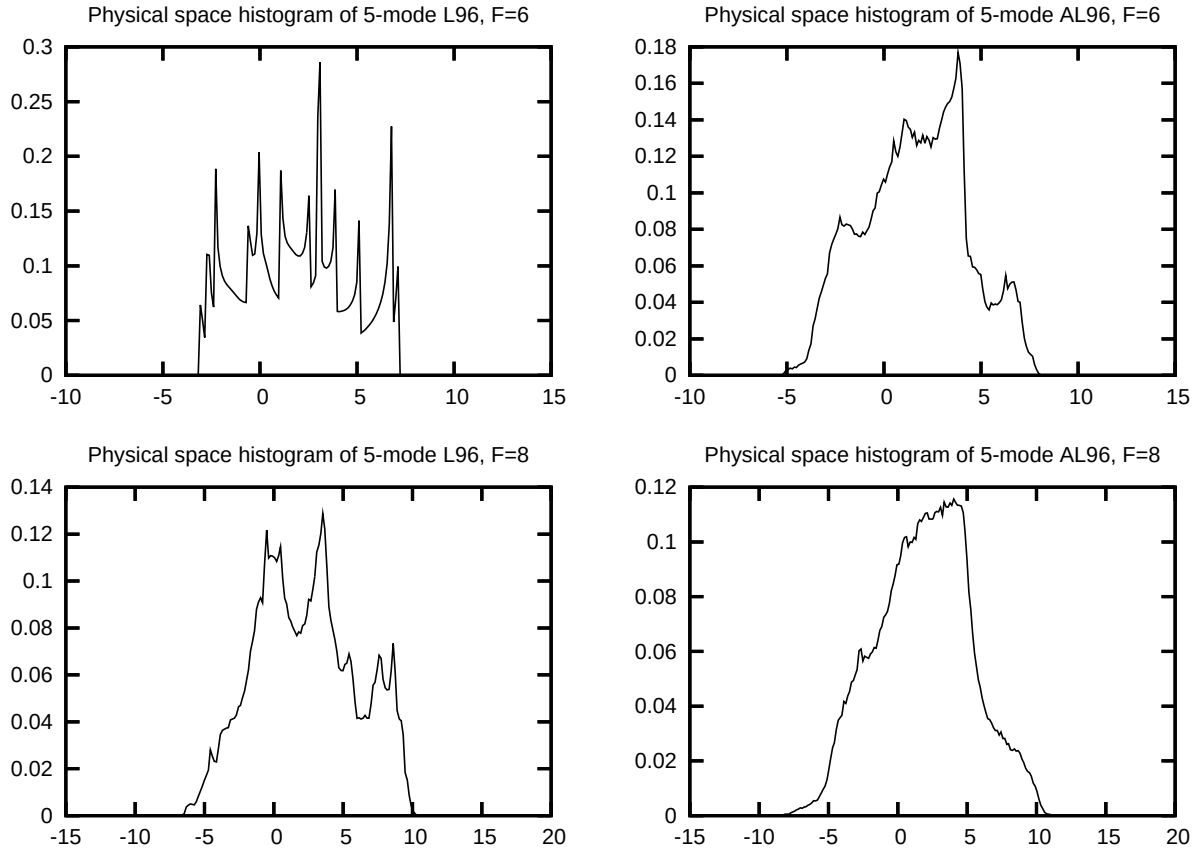

Figure 3.1: The probability density functions for the 5-mode L96 and AL96 models, dynamical regimes with constant forcing F set to 6 and 8.

3.1 and 3.2. Here the PDFs differ significantly depending on the value of forcing F. For $F = 6$, the multi-peaked PDF for the L96 model clearly exhibits quasi-periodic behavior, whereas the PDF for the AL96 model in the same dynamical regime provides evidence of mixing behavior, due to the absence of multiple sharp peaks. As F increases, none of the two models demonstrate quasi-periodic behavior, although the PDF for the AL96 model appears smoother than for the L96 model.

3.3 Time autocorrelation functions and correlation times

In this section we study mixing behavior of the 5-dimensional L96 and AL96 models through their time correlation functions. The time autocorrelation function $\mathcal{C}(\tau)$ of a phase space variable $x(t)$ is defined as a time average

$$\mathcal{C}(\tau) = \lim_{t\to\infty} \frac{1}{T} \int_{T_0}^{T_0+T} (x(t+\tau) - \bar{x})(x(t) - \bar{x}) \mathrm{d}t, \tag{3.7}$$

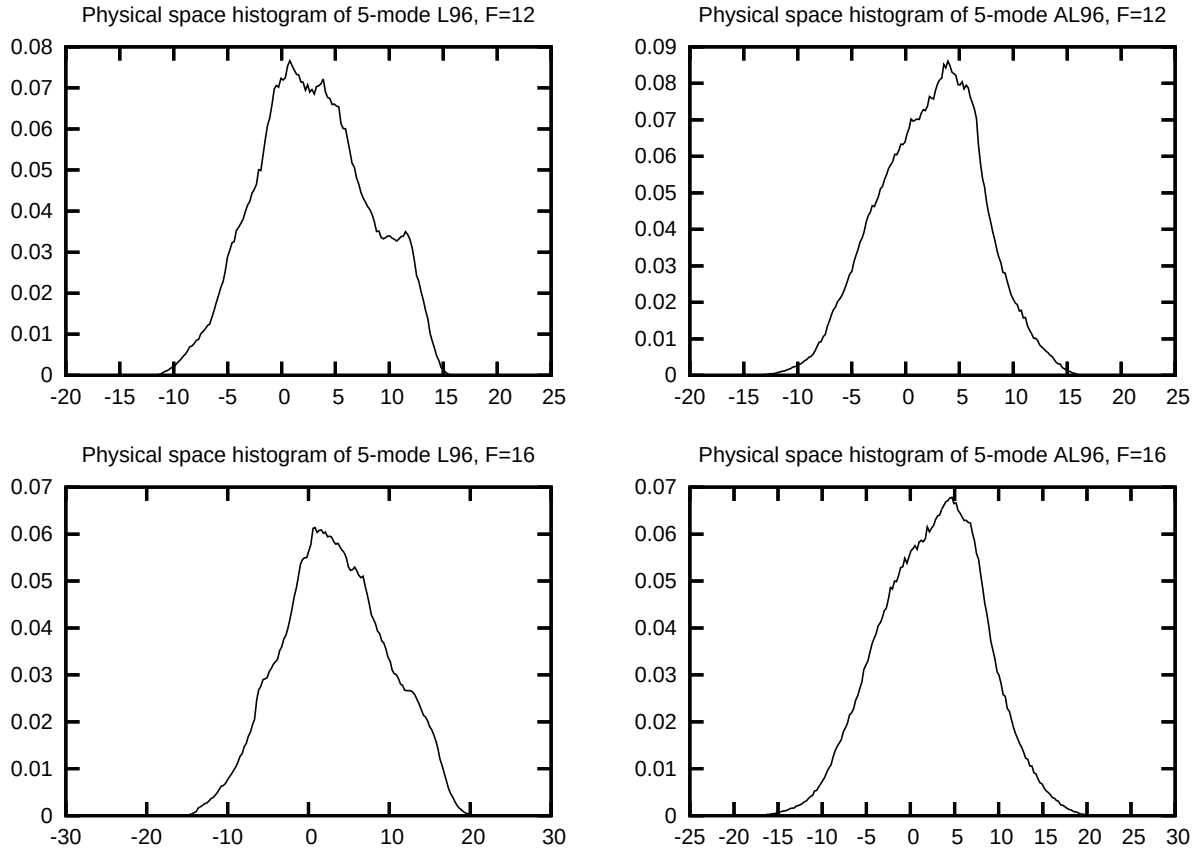

Figure 3.2: The probability density functions for the 5-mode L96 and AL96 models, dynamical regimes with constant forcing F set to 12 and 16.

and its decay rate serves as a measure of mixing behavior, or, alternatively, of the time interval over which a dynamical system "forgets" about its past state: the faster the decay of the correlation function in (3.7), the stronger mixing behavior the model exhibits. Mixing behavior is extremely important in applications where long time averages of various quantities have to be computed; weak mixing behavior (longer decay of autocorrelation functions) generally requires extremely long time averaging windows to achieve desired measurement precision. The typical time of decay of the correlation function is referred to as the correlation time. We distinguish between two types of correlation times: one is the time integral over the correlation function,

$$T_{corr} = \int_0^\infty \mathcal{C}(\tau)\mathrm{d}\tau, \tag{3.8}$$

while another is the time integral over the absolute value of the correlation function,

$$T_{|corr|} = \int_0^\infty |\mathcal{C}(\tau)|\mathrm{d}\tau. \tag{3.9}$$

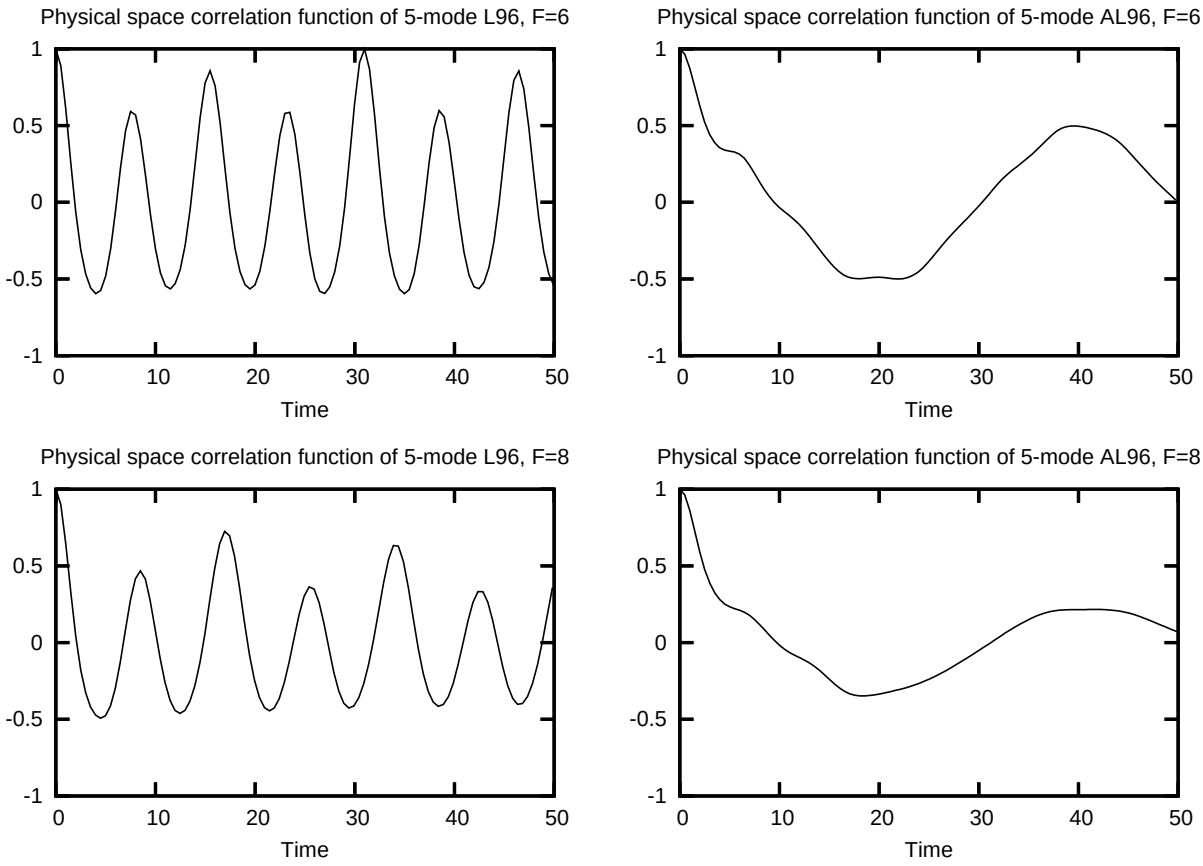

Figure 3.3: The time autocorrelation functions for the 5-mode L96 and AL96 models, dynamical regimes with constant forcing F set to 6 and 8.

The reason why two types of correlation functions are introduced is that, in the case of highly oscillatory slowly decaying time autocorrelation function (for example, for a quasi-periodic weakly mixing behavior), T_{corr} fails to capture slow decay due to self-canceling oscillations of the time autocorrelation function around zero, whereas $T_{|corr|}$ is not affected by oscillations and registers slow decay in such a case.

Here we display the time autocorrelation functions $\mathcal{C}(t)$ of the phase space variable for both L96 and AL96 models, as well as their correlation times. The time autocorrelation functions for the values of forcing $F = 6, 8, 12, 16$ are shown in Figures 3.3 and 3.4. The time scale in Figures 3.3 and 3.4 is renormalized so that the mean energy in new coordinates is 1 (for details, see [16]). Observe that for the L96 model in the dynamical regime $F = 6$ the time autocorrelation function does not visibly decay, which confirms strong evidence of quasi-periodic behavior of the L96 model for this regime. On the other hand, the time autocorrelation function of the AL96 model for the same regime exhibits decay, which means that the AL96 model for the $F = 6$ regime retains mixing behavior. For the rest of the dynamical regimes, $F = 8, 12, 16$, both L96 and AL96 models appear to be mixing, however

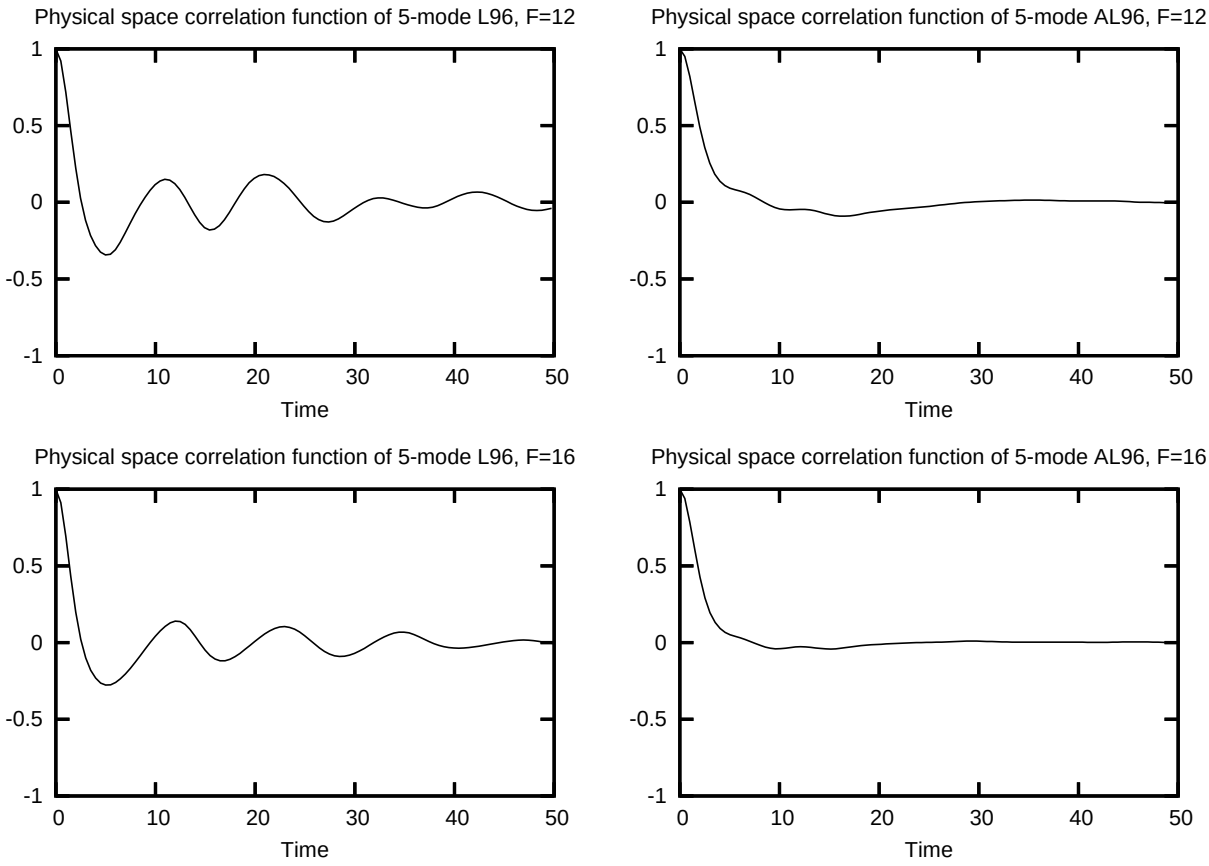

Figure 3.4: The time autocorrelation functions for the 5-mode L96 and AL96 models, dynamical regimes with constant forcing F set to 12 and 16.

the AL96 model shows much stronger mixing, which is, in fact, quite remarkable for such a low-dimensional model.

The correlation times for the physical space variables are shown in Table 3.3. Note significant discrepancies between T_{corr} and $T_{|corr|}$ for weakly mixing regimes for the L96 model, confirming the trends observed in Figures 3.3 and 3.4.

Overall, the statistical study of the 5-dimensional L96 and AL96 models suggests the following observations: first, both the L96 and AL96 models have two positive Lyapunov characteristic exponents in the forcing regimes $F = 6, 8, 12, 16$, which formally signifies chaotic behavior for both models in all studied dynamical regimes. Moreover, the L96 model generally possesses greater Lyapunov exponents, and thus a small uncertainty in initial conditions should develop faster in time for the L96 model. However, the trends in mixing behavior are entirely opposite. The AL96 model appears to have strongly mixing behavior in all studied dynamical regimes, whereas the L96 model is not mixing in the dynamical regime $F = 6$, and relatively weakly mixing in the regimes $F = 8, 12, 16$, which generally makes it less suitable for the test study of various approximations of the fluctuation-dissipation

	T_{corr}	$T_{\|corr\|}$
L96, $F = 6$	0.4083	∞
AL96, $F = 6$	2.996	16.47
L96, $F = 8$	-0.5091	∞
AL96, $F = 8$	1.957	10.91
L96, $F = 12$	0.3323	5.598
AL96, $F = 12$	1.621	3.563
L96, $F = 16$	0.3534	4.646
AL96, $F = 16$	1.806	2.598

Table 3.3: The correlation times for the 5-mode L96 and AL96 model, dynamical regimes corresponding to constant forcing F set to $6, 8, 12$ and 16. The $T_{|corr|}$ correlation times for the L96 model in the regimes $F = 6, 8$ are marked as ∞ due to the fact that no decay of oscillations has been registered for as long as the the autocorrelation functions could be practically computed.

theorem.

4 Numerical testing of different FDT approximations with the 5-mode AL96 model

The ability of the 5-mode AL96 model to be mixing even in the weakly chaotic regimes $F = 6, 8$, discovered in Section 3, makes it an ideal testbed to study the linear response for different FDT methods. Here we study the linear response of the two novel FDT methods, ST-FDT and hA-FDT, compare them with the classical qG-FDT response and validate their performance against the so-called "ideal response" operator, R_{ideal}, which is the actual directly measured response of the model, perturbed by series of small external forcing perturbations. To compute the ideal response, these small perturbations are applied to a large statistical ensemble of solutions ($\sim$ 100000 members) to ensure sufficient precision in measuring the mean linear response. This ideal response operator has been developed by Gritsoun and Dymnikov [10], and has been used for validation of classical FDT response for various chaotic dynamical systems in [16]. For extensive description and numerical algorithms for the ideal response operator, see [10, 16]. The numerical parameters for FDT simulations for the AL96 model essentially follow those used in the climatological study of the L96 and AL96 models in Section 3:

- Anti Lorenz 96 (AL96) model from (3.3);
- Dimension of the model $N = 5$;
- Two different vector-valued response functions are studied: linear response function $\vec{A}(\vec{x}) = \vec{x}$, and nonlinear response function $A_i(\vec{x}) = x_i^2$;

- Values of forcing $F = 6, 8, 12, 16$;
- 4th order Runge-Kutta time integrator;
- Discrete time step $\Delta t = 1/64$;
- Time averaging window for qG-FDT, ST-FDT and hA-FDT responses is $T = 500000$ time units;
- Spin-up time $T_0 = 10000$ time units is skipped before computing averages to let the numerical trajectory land on the attractor;
- The response is measured for constant small external forcing;
- Ensemble size for the ideal response is 100000 members.

As stated above, all response operators are computed for constant small external perturbations, and therefore we display the qG-FDT, ST-FDT and hA-FDT linear response operators from formulas (2.34), (2.26) and (2.43), respectively, rather than their convolution kernels in more general formulas for arbitrary time- and space-dependent external perturbations. Also observe that while the theory in Section 2 is developed for a scalar response function $A(\vec{x})$, the tested response functions above are vector-valued. As a result, the linear response operator $R(\tau)$ becomes a matrix, rather than being vector in Section (2), which is a simple and straightforward generalization of scalar linear response function onto vector-valued response. However, since the AL96 model is translationally invariant (given its periodic boundary conditions), the columns of all linear response operators translate into each other along the main diagonal. Thus, rather than displaying linear response operators as matrices with translationally invariant columns, we show their middle (i.e. 3rd for $N = 5$) columns, which correspond for response to unit external forcing at the middle coordinate. This is done to aid visualization and simplify comparative analysis of performance for different response operators. Additionally, validation of ideal response operators is done at the end of Section 4. The time scale for linear response measurements is appropriately rescaled by the energy of perturbations like in Chapter 2 of [16], to ensure consistent response time scales for different dynamical regimes regardless of their mean energy.

Quantification of errors In addition to visual representation of discrepancy between the ideal response operators and different FDT linear response operators, we need a systematic way to quantify these errors. There are two distinct aspects of error quantification.

- The first aspect, which is the most obvious, is a bulk error between responses computed at different coordinates x_j for a given forcing, which can be quantified by a simple error norm, for example, Euclidean L_2-norm. The L_2-error between an FDT and ideal operator is defined as
$$L_2\text{-error} = \frac{\|R_{FDT} - R_{ideal}\|}{\|R_{ideal}\|}, \tag{4.1}$$
where $\|\cdot\|$ denotes the norm generated by the standard Euclidean inner product.

- The second, less obvious aspect, is the similarity, or physical correlation between two response operators, which signifies the error in location of a response, rather than its strength. In a number of practical geophysical applications, predicting the correct location of some phenomena is often more important than predicting their magnitude at the same location [9]. In order to address the physical correlation, or similarity, between the two responses, we introduce a special physical space correlation function, which is defined as

$$Corr = \frac{(R_{FDT}, R_{ideal})}{\|R_{FDT}\|\|R_{ideal}\|}, \tag{4.2}$$

  where $(\cdot,\cdot)$ is the standard Euclidean inner product. Thus, the L_2-error as defined in (4.1) indicates the bulk discrepancy between the FDT and ideal operators, whereas the $Corr$ function as defined in (4.2) signifies the collinearity of the two operators. The value of 1 of the $Corr$ function indicates complete collinearity between the two operators (without the regard of their magnitudes, which could be very different), and the value of 0 indicates complete decorrelation. Negative values of the physical correlation function provide the evidence that the two responses are anti-correlated.

Both methods of error estimation are utilized to capture different aspects of approximation by the various FDT approximations to the ideal response.

4.1 Comparison of FDT methods for a linear response function

Here we compare different methods for FDT linear response for a simple vector-valued response function

$$\vec{A}(\vec{x}) = \vec{x}. \tag{4.3}$$

The response function in (4.3) corresponds to the mean state response to external fluctuation, which is a key basic climatological property of a geophysical system. Since the response to constant small external forcing is used, we compute the qG-FDT, ST-FDT and hA-FDT linear response operators from formulas (2.34), (2.26) and (2.43), respectively. The profiles for the response operators at times $T = 2, 5, 10$ and 20 (where time is counted from the moment the constant forcing is turned on) for dynamical regimes $F = 6, 8, 12, 16$ are shown in Figures 4.1, 4.2, 4.3 and 4.4, respectively. Note that, since the response function is vector-valued, all linear response operators are matrices. However, due to translational invariance of the AL96 model, all columns of response operators are translations of the first column. To avoid confusion, we display a graph of the middle column for each response operator, which, essentially, is the normalized response to small fluctuation at a central discretization point. Here one may observe different trends in quality of approximation for different dynamical regimes. The ST-FDT method is clearly better than both qG-FDT and hA-FDT for shorter times, $T = 2$ and $T = 5$, for all displayed dynamical regimes $F = 6, 8, 12, 16$. However, as predicted above in Section 2, for longer time $T = 10$, ST-FDT rapidly loses precision, and for the longest time, $T = 20$ it is not displayed due to exponential growth of the tangent map in expanding directions and eventual numerical blowup. The hA-FDT method appears to be superior to the classical qG-FDT method for longer times, $T = 10$ and $T = 20$, especially in

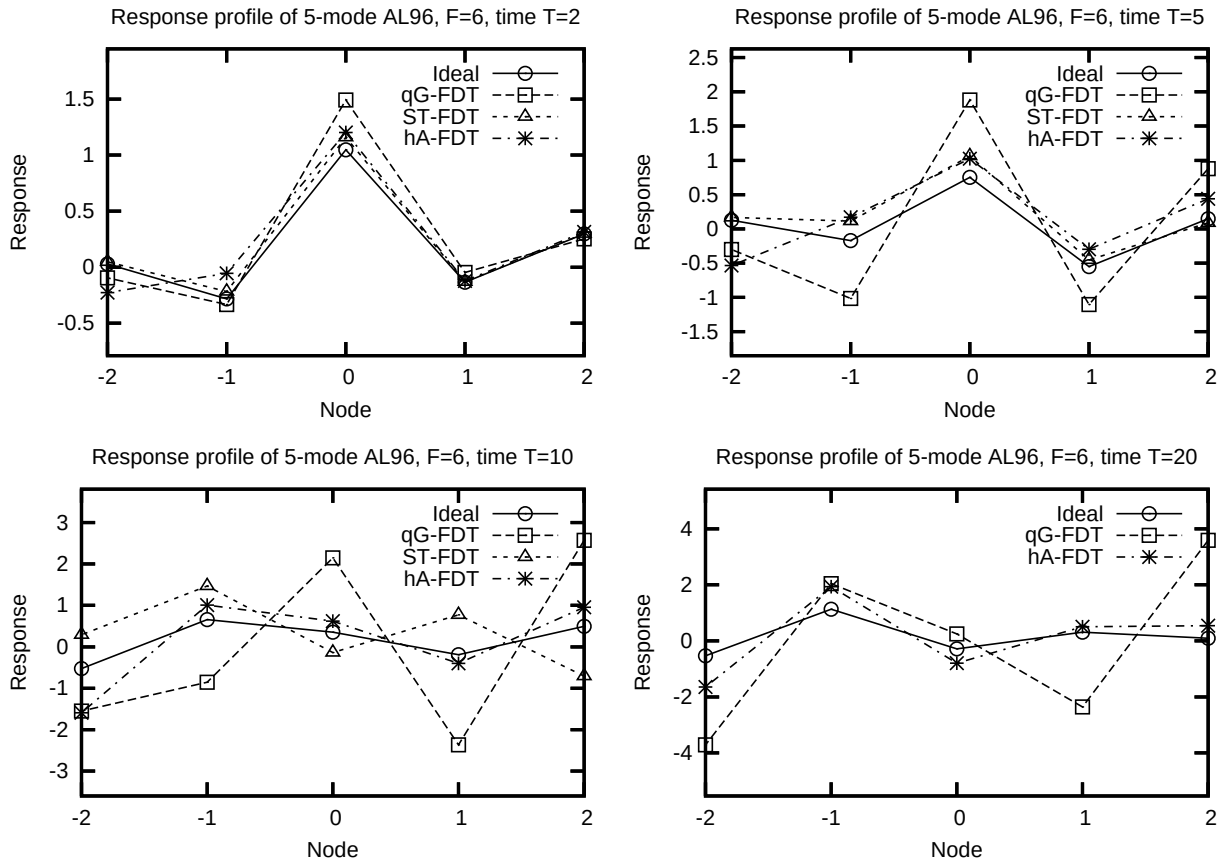

Figure 4.1: Snapshots of the response operators for linear response function $\vec{A}(\vec{x}) = \vec{x}$ at time $T = 2, 5, 10, 20$ for the 5-mode AL96 model, $F = 6$.

the weakly chaotic regime $F = 6$ (where the quasi-Gaussian approximation is not expected to work well). For more chaotic dynamical regimes, $F = 8, 12, 16$, the superiority of the hA-FDT over qG-FDT for longer times tends to diminish, which can be explained by the fact that the classical qG-FDT approximation becomes more robust as the dynamical regime becomes more chaotic (for extensive details see Chapter 2 of [16]).

In addition to displaying the response operator profiles in Figures 4.1, 4.2, 4.3 and 4.4, we also summarize the L_2-errors of the qG-FDT, ST-FDT, and hybrid A-FDT operators in Table 4.1, whereas their physical correlations are displayed in Table 4.2. One can observe that the ST-FDT method is superior to both qG-FDT and hA-FDT methods for times $T = 2$ and $T = 5$, both in L_2-error, where the improvement is 2-3 times compare to hA-FDT and qG-FDT (Table 4.1) and physical correlation (Table 4.2). As for the hA-FDT method, it produces smaller errors (by a factor of 3-4) than the qG-FDT method in the weakly chaotic dynamical regime $F = 6$ for all times $T = 2, 5, 10, 20$, and better physical correlation with the ideal response in the same regimes for $T = 2, 10, 20$. In the regime $F = 8$ the hA-FDT produces smaller errors for all times (by a factor of 2-3) than the qG-FDT method, however the qG-FDT method produces slightly better correlation (although both methods are fairly

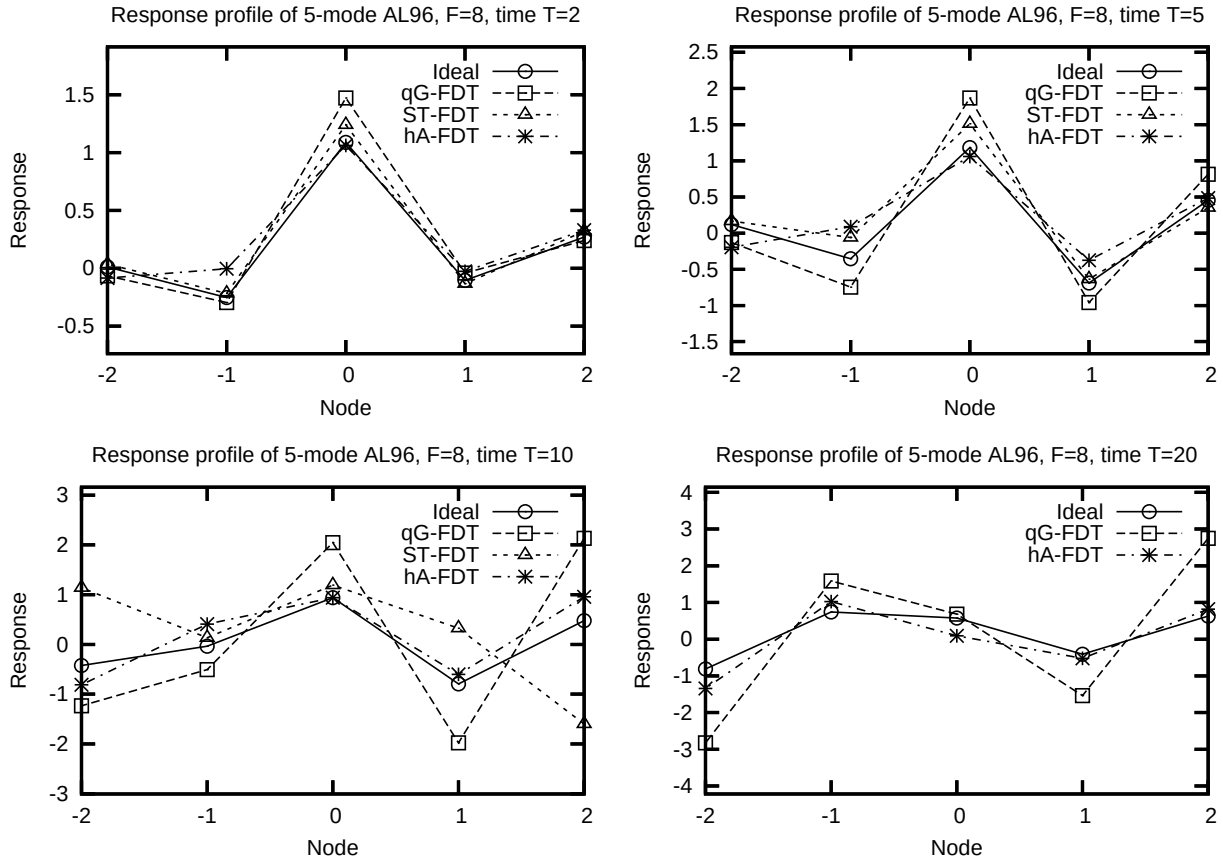

Figure 4.2: Snapshots of the response operators for linear response function $\vec{A}(\vec{x}) = \vec{x}$ at time $T = 2, 5, 10, 20$ for the 5-mode AL96 model, $F = 8$.

well correlated). For more chaotic dynamical regimes $F = 12$ and $F = 16$, the hA-FDT method produces smaller errors (by 20-30%) for longer times $T = 10$ and $T = 20$, but, like for the $F = 8$ regimes, the physical correlation with the ideal response is better for the qG-FDT method.

Overall, the three methods have cleanly defined advantages before each other: the ST-FDT method is superior in all respects but for short times, the hA-FDT dominates in dynamical regimes with weaker chaos for longer times, whereas the qG-FDT tends to perform better in strongly chaotic regimes for longer times.

4.2 Comparison of FDT results for a quadratic response function

Here we compare different methods for FDT linear response for a simple quadratic vector-valued response function

$$A_i(\vec{x}) = x_i^2, \tag{4.4}$$

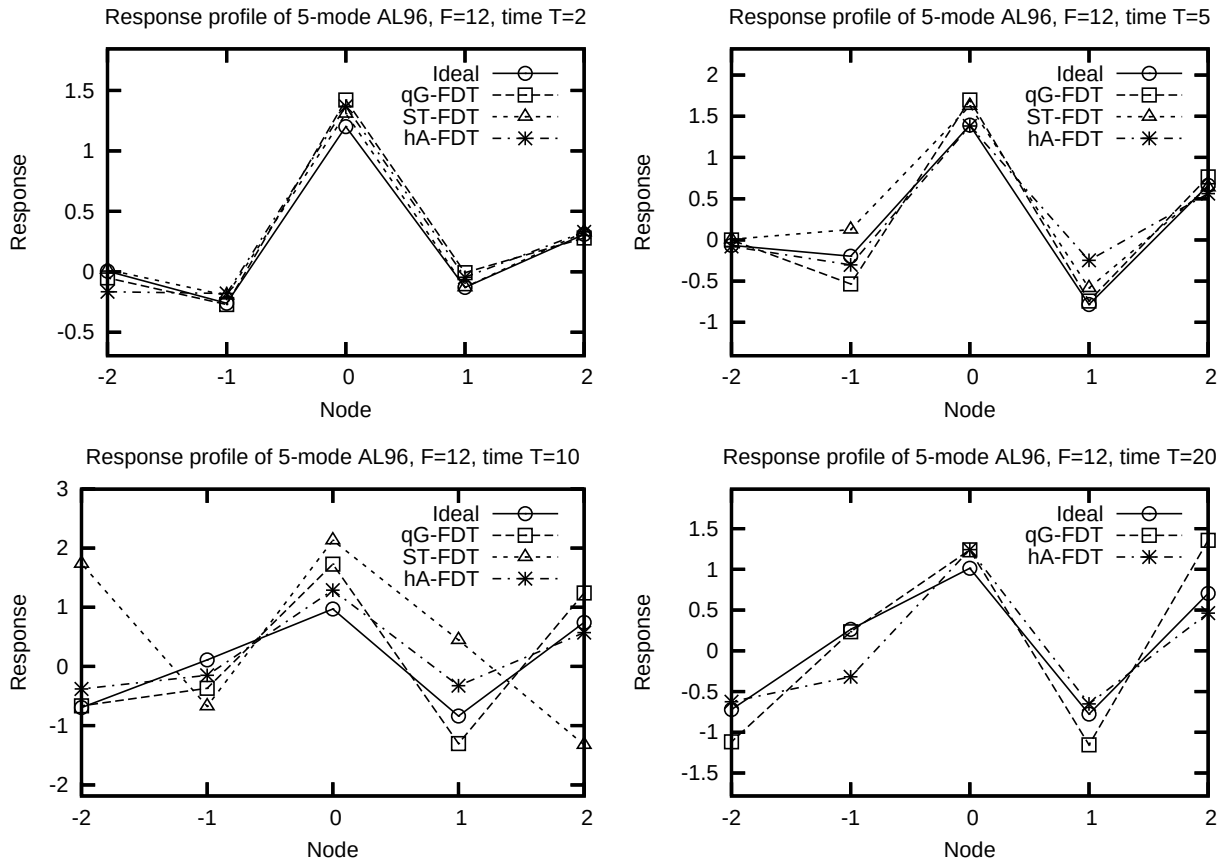

Figure 4.3: Snapshots of the response operators for linear response function $\vec{A}(\vec{x}) = \vec{x}$ at time $T = 2, 5, 10, 20$ for the 5-mode AL96 model, $F = 12$.

where each component of the response vector $\vec{A}$ is obtaining by raising the corresponding component of $\vec{x}$ to the second power. The response function in (4.4) corresponds to the response of the variance of the mean state to external fluctuation, which is, like the mean state itself, an important climatological property of a geophysical system. Since the response to constant small external forcing is used, we compute the qG-FDT, ST-FDT and hA-FDT linear response operators from formulas (2.34), (2.26) and (2.43), respectively. The profiles for the response operators at times $T = 2, 5, 10$ and 20 for dynamical regimes $F = 6, 8, 12, 16$ are shown in Figures 4.5, 4.6, 4.7 and 4.8, respectively. Note that, as in the previous section, we display a graph of the middle column for each response operator, which, essentially, is the normalized response to small fluctuation at a central discretization point. Here the trends in quality of approximation for different dynamical regimes are similar to those for the response function of the mean state in Section 4.1. The ST-FDT method is clearly better than both qG-FDT and hA-FDT for shortest time, $T = 2$, for all displayed dynamical regimes $F = 6, 8, 12, 16$. However, as predicted above in Section 2, for longer times $T = 5, 10$, ST-FDT rapidly loses precision, and for the longest time, $T = 20$ it is not displayed due to exponential growth of the tangent map in expanding directions and eventual numerical

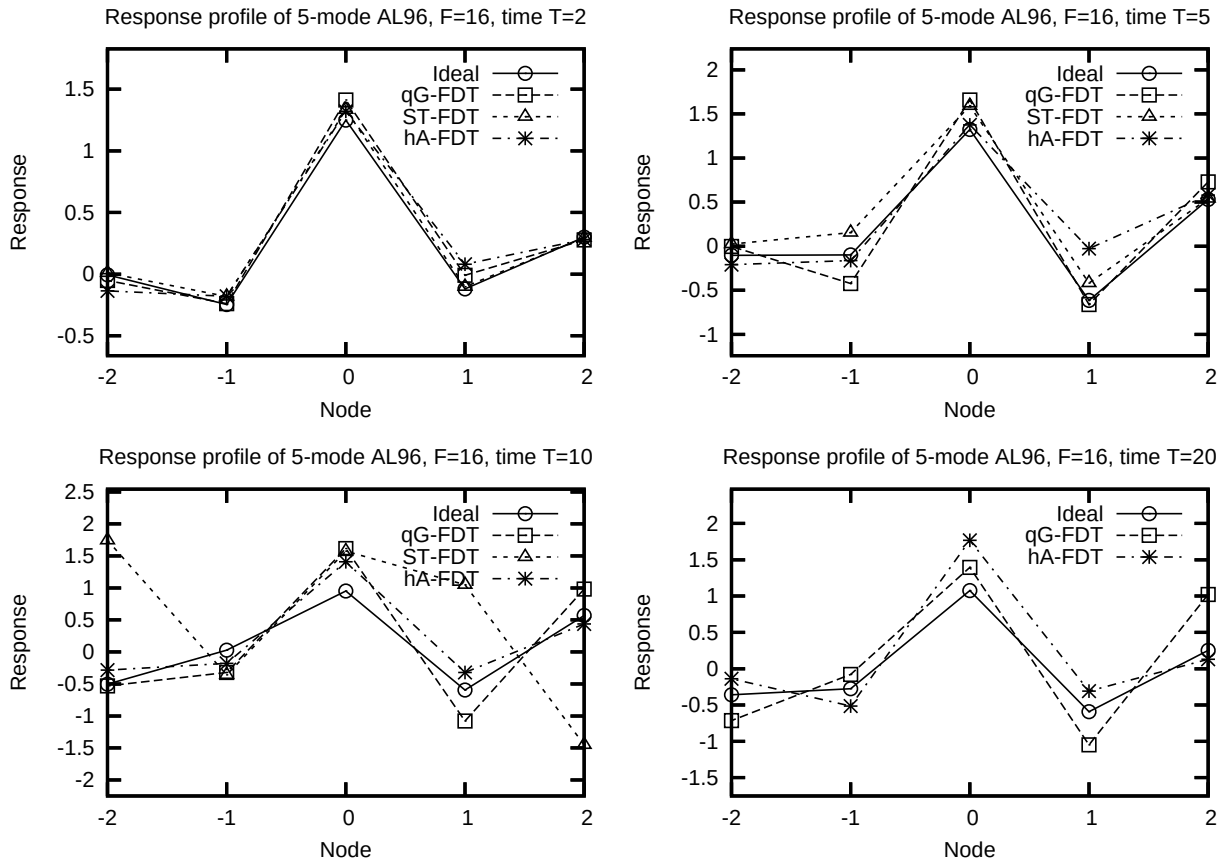

Figure 4.4: Snapshots of the response operators for linear response function $\vec{A}(\vec{x}) = \vec{x}$ at time $T = 2, 5, 10, 20$ for the 5-mode AL96 model, $F = 16$.

blowup. The hA-FDT method appears to be superior to the classical qG-FDT method for all times, $T = 2, 5, 10, 20$, in the weakly and moderately chaotic regimes $F = 6$ and $F = 8$. For more chaotic dynamical regimes, $F = 12$ and $F = 16$, qG-FDT is generally better than hA-FDT.

In addition to displaying the response operator profiles in Figures 4.5, 4.6, 4.7 and 4.8, we also summarize the L_2-errors of the qG-FDT, ST-FDT, and hybrid A-FDT operators in Table 4.3, whereas their physical correlations are displayed in Table 4.4. One can observe that the ST-FDT method is superior to both qG-FDT and hA-FDT methods for the shortest time $T = 2$ both in L_2-error, by a factor of 3-4 (Table 4.3), and physical correlation (Table 4.4). As for the hA-FDT method, it produces smaller errors (by a factor of 2-3) than the qG-FDT method in the weakly and moderately chaotic dynamical regimes $F = 6$ and $F = 8$ for all times $T = 2, 5, 10, 20$, and better physical correlation with the ideal response in the same regimes for all times. For more chaotic dynamical regimes $F = 12$ and $F = 16$, the qG-FDT method produces smaller errors and better correlations than the hA-FDT method.

Like in Section 4.1, here for the quadratic response function the three methods have

Response L_2-error values of 5-mode AL96, F=6			
Time	qG-FDT	ST-FDT	hA-FDT
2	0.4188	0.1168	0.3329
5	1.791	0.4536	0.9107
10	3.731	1.881	1.189
20	4.186	21.07	1.169
Response L_2-error values of 5-mode AL96, F=8			
Time	qG-FDT	ST-FDT	hA-FDT
2	0.3471	0.1451	0.2479
5	0.632	0.3074	0.4294
10	1.804	2.053	0.5643
20	2.241	73.6	0.556
Response L_2-error values of 5-mode AL96, F=12			
Time	qG-FDT	ST-FDT	hA-FDT
2	0.2036	0.09942	0.2087
5	0.2719	0.2611	0.3191
10	0.6862	2.264	0.4561
20	0.5339	56.86	0.4186
Response L_2-error values of 5-mode AL96, F=16			
Time	qG-FDT	ST-FDT	hA-FDT
2	0.1559	0.08353	0.1977
5	0.3326	0.2801	0.3878
10	0.7242	2.595	0.4632
20	0.7755	127.5	0.6186

Table 4.1: L_2-errors of linear response operators with ideal operator for linear response function $\vec{A}(\vec{x}) = \vec{x}$, time $T = 2, 5, 10, 20$ for the 5-mode AL96 model, $F = 6, 8, 12, 16$.

cleanly defined advantages compared with each other: the ST-FDT method is superior in all respects for sufficiently short times, the hA-FDT dominates in dynamical regimes with weaker chaos for longer times, whereas the qG-FDT tends to perform better in strongly chaotic regimes for longer times.

4.3 Linearity validation for the ideal response

To confirm the validity of the results above, we need to ensure that the ideal response itself is sufficiently linear. The reason why it can be nonlinear (mainly for longer times) is because, as outlined above in the beginning of this section, the ideal response is the actual measured response of nonlinear dynamics to small external forcing, developed by Gritsoun and Dymnikov [10]. Thus, in order for the ideal response to exhibit linearity, the external forcing, from which it is measured, must be sufficiently small. In order to

Response $Corr$ values of 5-mode AL96, F=6			
Time	qG-FDT	ST-FDT	hA-FDT
2	0.9862	0.9967	0.9572
5	0.9175	0.9339	0.7264
10	0.5811	0.1362	0.9599
20	0.4789	0.2736	0.9574
Response $Corr$ values of 5-mode AL96, F=8			
Time	qG-FDT	ST-FDT	hA-FDT
2	0.993	0.9983	0.9688
5	0.9856	0.966	0.906
10	0.9592	−0.1212	0.8965
20	0.9391	−0.8635	0.9297
Response $Corr$ values of 5-mode AL96, F=12			
Time	qG-FDT	ST-FDT	hA-FDT
2	0.9927	0.998	0.9872
5	0.9843	0.9695	0.9498
10	0.9616	−0.1095	0.8903
20	0.9839	−0.9231	0.9118
Response $Corr$ values of 5-mode AL96, F=16			
Time	qG-FDT	ST-FDT	hA-FDT
2	0.9947	0.998	0.9822
5	0.9843	0.9708	0.9231
10	0.9767	−0.21	0.9144
20	0.9289	−0.1047	0.923

Table 4.2: Physical correlations of linear response operators with ideal operator for linear response function $\vec{A}(\vec{x}) = \vec{x}$, time $T = 2, 5, 10, 20$ for the 5-mode AL96 model, $F = 6, 8, 12, 16$.

ensure sufficient linearity of the ideal response, we compare two ideal responses measured for two different magnitudes of external forcing (for details, see Chapter 2 of [16]). The error between these two ideal responses is, thus, directly related to nonlinearity in the ideal response. Here we choose two magnitudes of small external forcing for computing the ideal response: $\delta f_1 = 0.02F$ and $\delta f_2 = 0.05F$, where F is the constant forcing parameter in (3.3).

In addition to displaying the response operator profiles for comparison, we also compute the L_2-errors between two ideal responses. The L_2-error between two ideal response operators R_1 and R_2 is defined as in (4.1).

Here, for simplicity in exposition, we only report on the linearity of the ideal response for two dynamical regimes: the least chaotic and mixing $F = 6$ and the most chaotic and mixing $F = 16$. The profiles of the ideal responses are shown in Figures 4.9 and 4.10, for time snapshots $T = 2, 5, 10, 20$ (here the time is counted from the moment the external forcing has been turned on). As we can see, the two ideal responses with different external forcings

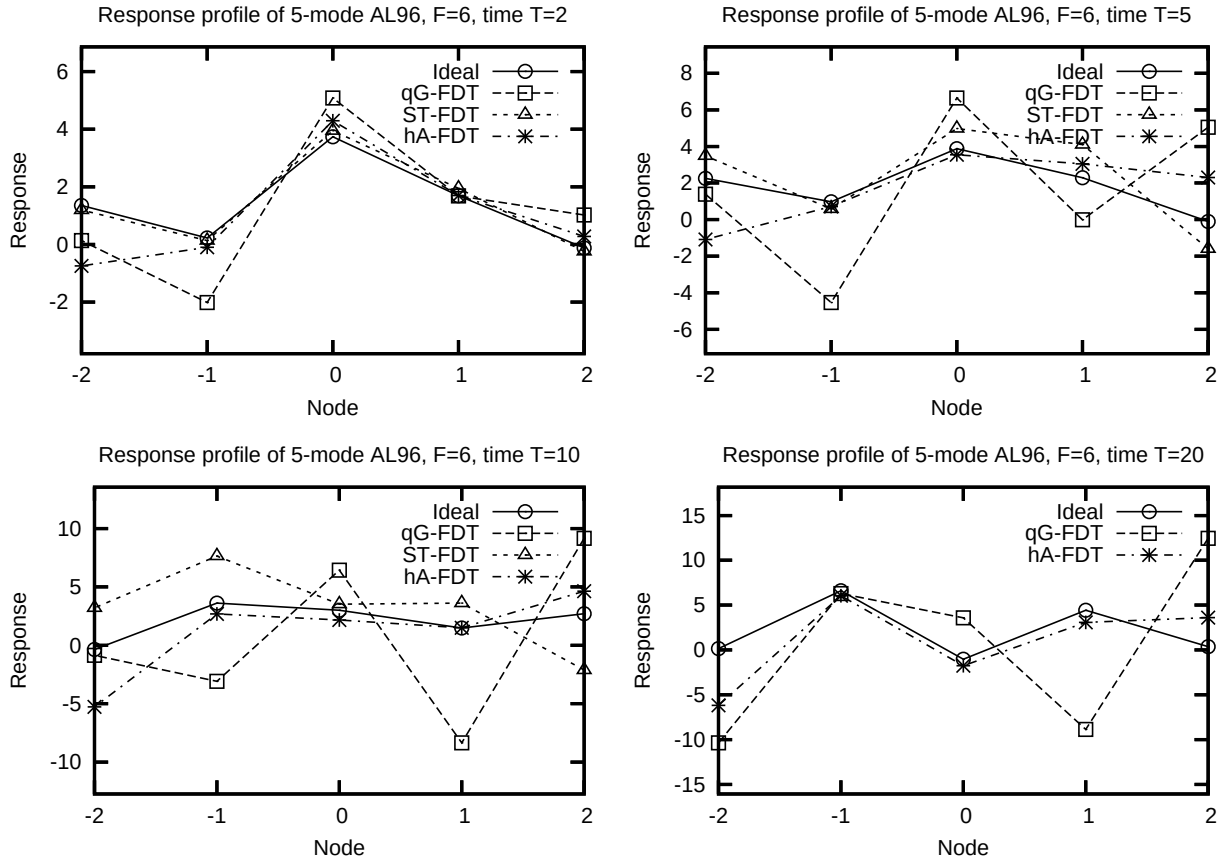

Figure 4.5: Snapshots of the response operators for quadratic response function $A_i(\vec{x}) = x_i^2$ at time $T = 2, 5, 10, 20$ for the 5-mode AL96 model, $F = 6$.

δf_1 and δf_2 visually match each other very well for both dynamical regimes $F = 6$ and $F = 16$. Only for the time $T = 20$ there is a slight visible discrepancy for both dynamical regimes. The L_2-errors for both regimes are recorded in Table 4.5. Here we can see that the errors between the two linear operators systematically grow in time, although even for the relatively long time, $T = 20$, the errors are small.

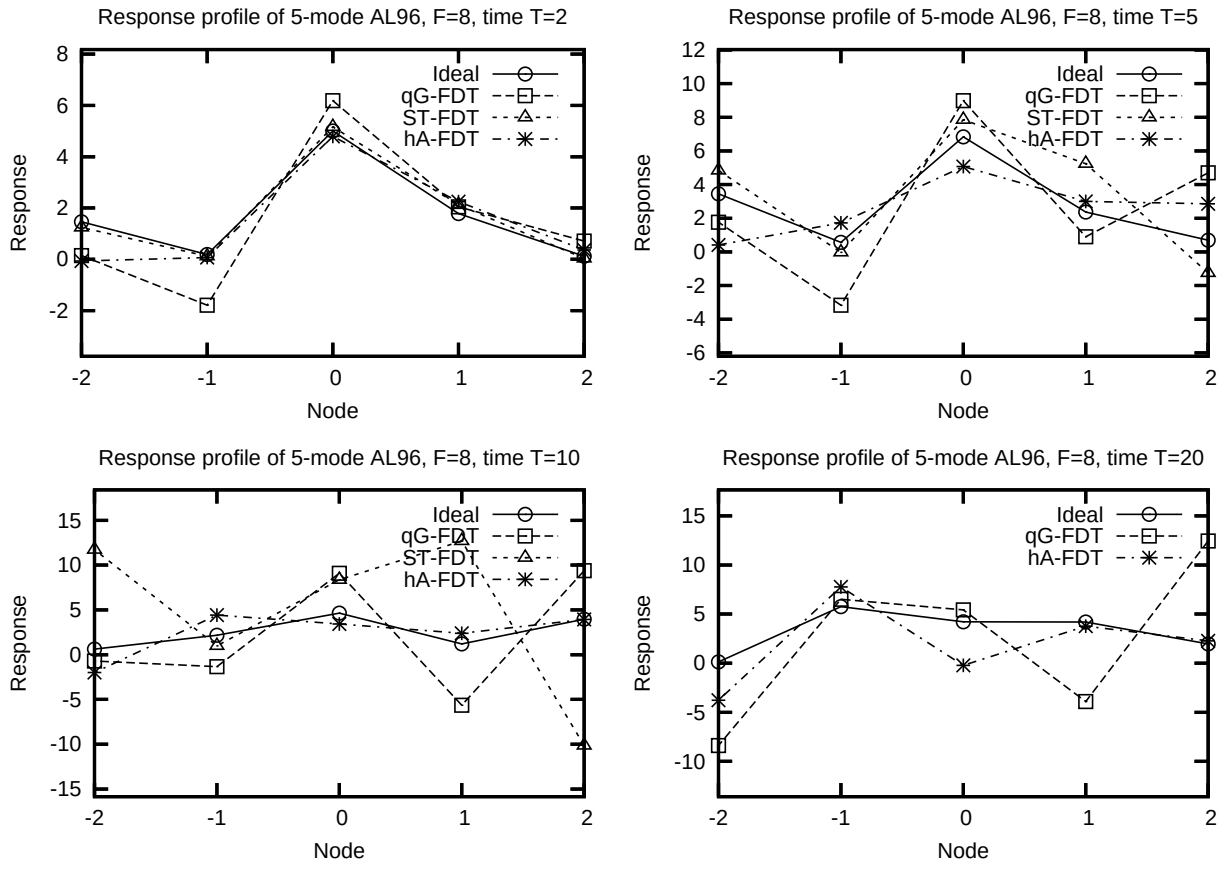

Figure 4.6: Snapshots of the response operators for quadratic response function $A_i(\vec{x}) = x_i^2$ at time $T = 2, 5, 10, 20$ for the 5-mode AL96 model, $F = 8$.

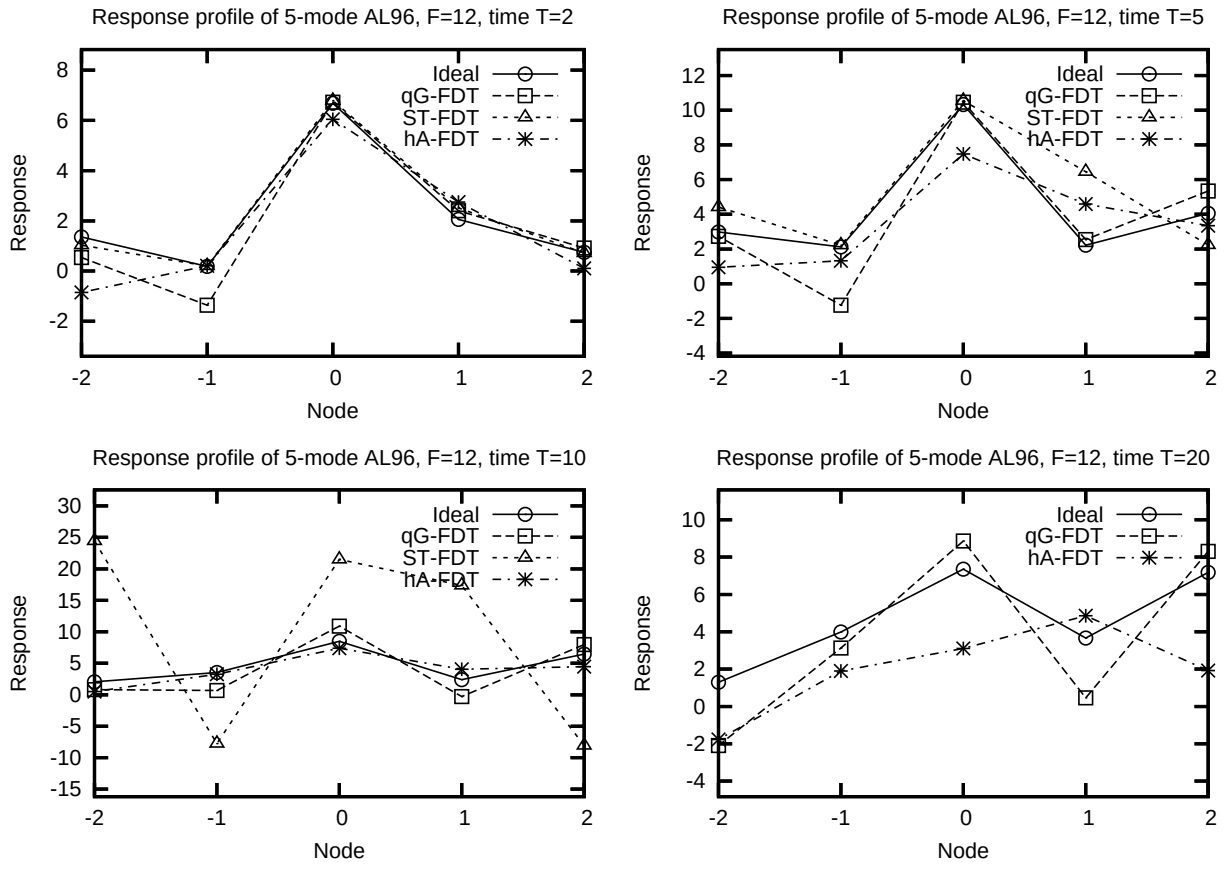

Figure 4.7: Snapshots of the response operators for quadratic response function $A_i(\vec{x}) = x_i^2$ at time $T = 2, 5, 10, 20$ for the 5-mode AL96 model, $F = 12$.

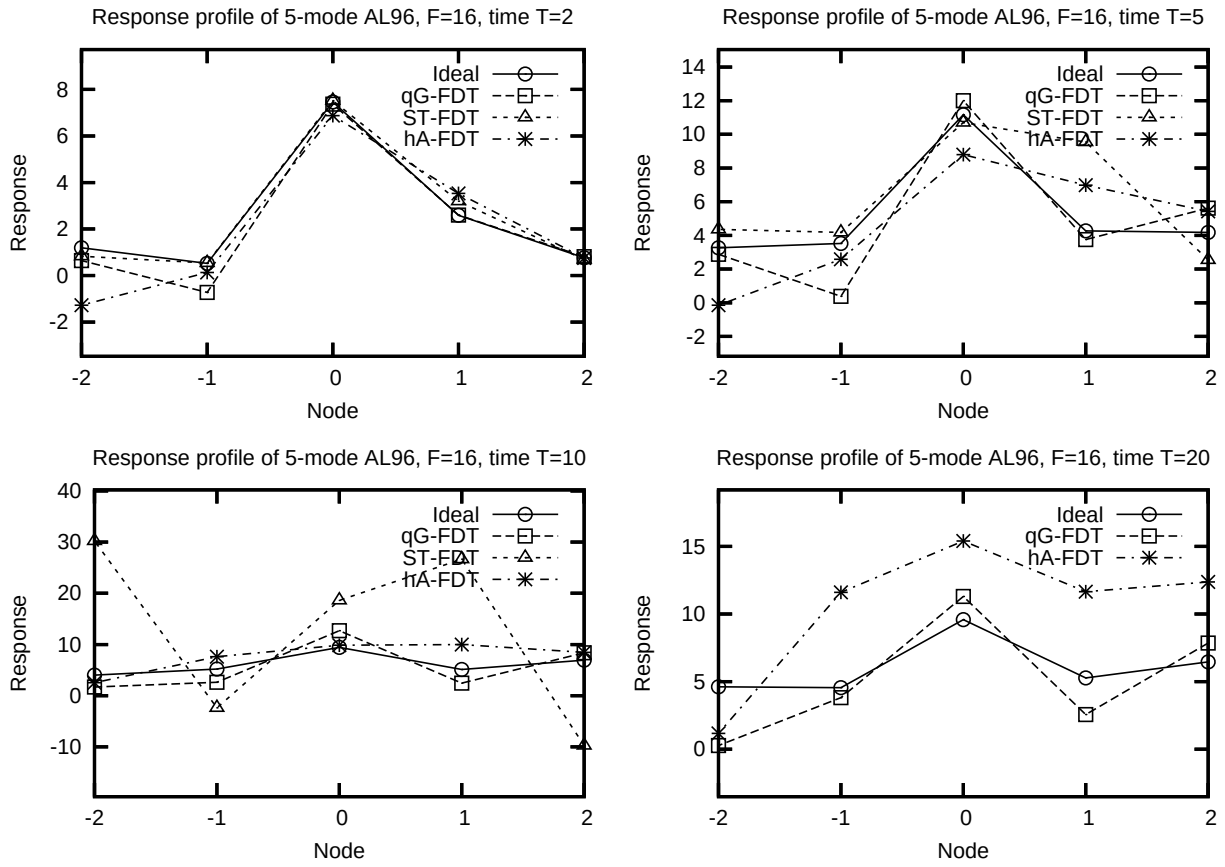

Figure 4.8: Snapshots of the response operators for quadratic response function $A_i(\vec{x}) = x_i^2$ at time $T = 2, 5, 10, 20$ for the 5-mode AL96 model, $F = 16$.

Response L_2-error values of 5-mode AL96, F=6			
Time	qG-FDT	ST-FDT	hA-FDT
2	0.7165	0.09131	0.5153
5	1.637	0.5644	0.8192
10	2.485	1.345	0.9635
20	2.659	28.16	0.9114

Response L_2-error values of 5-mode AL96, F=8			
Time	qG-FDT	ST-FDT	hA-FDT
2	0.496	0.08174	0.2955
5	0.7788	0.4857	0.5367
10	1.586	3.275	0.5814
20	1.857	156.9	0.734

Response L_2-error values of 5-mode AL96, F=12			
Time	qG-FDT	ST-FDT	hA-FDT
2	0.2501	0.08062	0.3471
5	0.3045	0.4064	0.3667
10	0.4291	3.01	0.2755
20	0.4362	103.7	0.6672

Response L_2-error values of 5-mode AL96, F=16			
Time	qG-FDT	ST-FDT	hA-FDT
2	0.1697	0.08898	0.3401
5	0.2671	0.4201	0.3839
10	0.3923	2.756	0.4081
20	0.3948	235.1	0.9176

Table 4.3: L_2-errors of linear response operators with ideal operator for quadratic response function $A_i(\vec{x}) = x_i^2$, time $T = 2, 5, 10, 20$ for the 5-mode AL96 model, $F = 6, 8, 12, 16$.

Response *Corr* values of 5-mode AL96, F=6			
Time	qG-FDT	ST-FDT	hA-FDT
2	0.8524	0.9975	0.8804
5	0.4872	0.9656	0.6803
10	0.2596	0.6545	0.7335
20	$1.007 \cdot 10^{-2}$	0.1127	0.6922

Response *Corr* values of 5-mode AL96, F=8			
Time	qG-FDT	ST-FDT	hA-FDT
2	0.9223	0.9975	0.9554
5	0.8165	0.9507	0.8438
10	0.7308	0.1625	0.8595
20	0.447	−0.07516	0.7713

Response *Corr* values of 5-mode AL96, F=12			
Time	qG-FDT	ST-FDT	hA-FDT
2	0.9698	0.9971	0.9378
5	0.9564	0.9353	0.9406
10	0.9319	0.4322	0.9667
20	0.9162	0.2351	0.7731

Response *Corr* values of 5-mode AL96, F=16			
Time	qG-FDT	ST-FDT	hA-FDT
2	0.9855	0.9965	0.9411
5	0.9664	0.9359	0.9235
10	0.9336	0.5407	0.9632
20	0.9235	0.05098	0.9461

Table 4.4: Physical correlations of linear response operators with ideal operator for quadratic response function $A_i(\vec{x}) = x_i^2$, time $T = 2, 5, 10, 20$ for the 5-mode AL96 model, $F = 6, 8, 12, 16$.

L_2-error values of 5-mode AL96, F=6	
Time	p=0.02F vs p=0.05F
2	$0.3316 \cdot 10^{-2}$
5	$1.034 \cdot 10^{-2}$
10	0.09133
20	0.1601

L_2-error values of 5-mode AL96, F=16	
Time	p=0.02F vs p=0.05F
2	$1.224 \cdot 10^{-3}$
5	$2.74 \cdot 10^{-2}$
10	0.1
20	0.1756

Table 4.5: L_2-errors between the ideal operators generated with small external perturbations of two different magnitudes, time $T = 2, 5, 10, 20$ for the 5-mode AL96 model, $F = 6$ and $F = 16$. Magnitudes of external perturbations are $\delta f_1 = 0.02F$ and $\delta f_2 = 0.05F$.

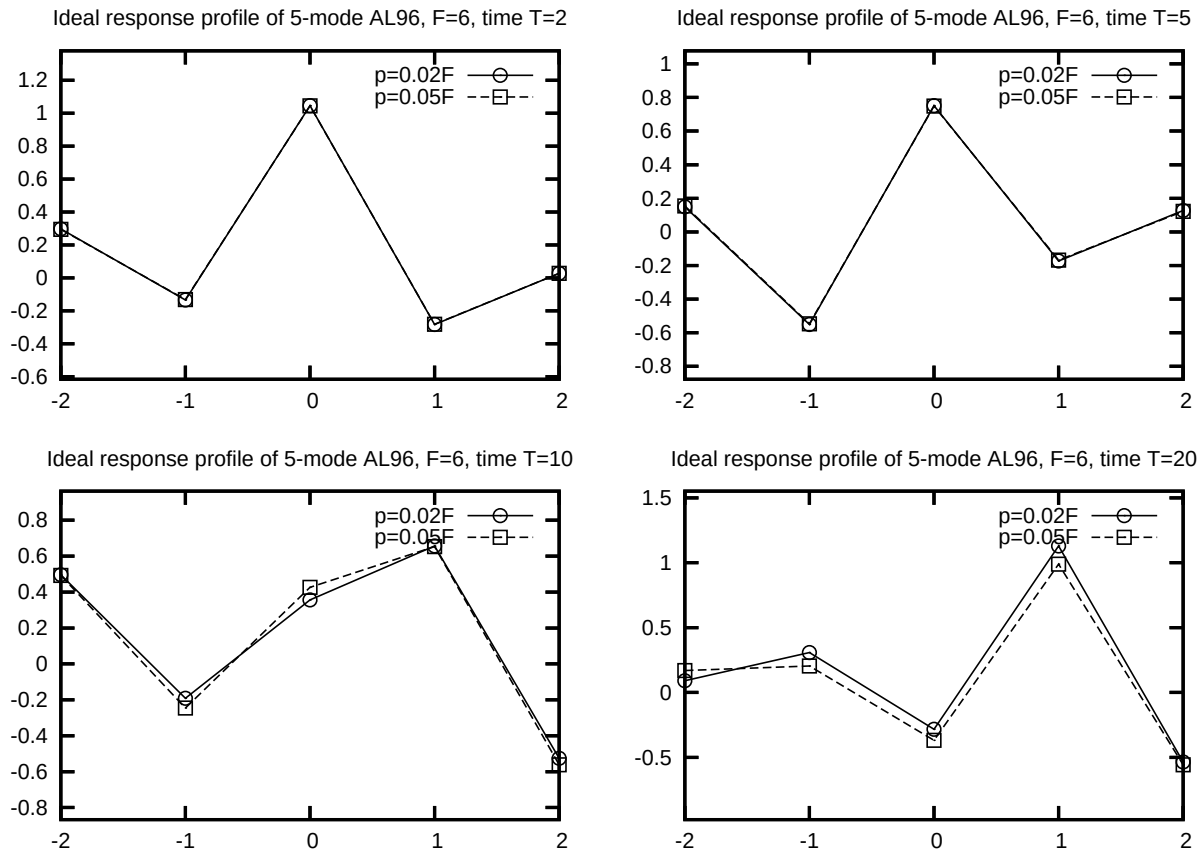

Figure 4.9: Snapshots of the ideal response operators at time $T = 2, 5, 10, 20$ for the 5-mode AL96 model, $F = 6$. Magnitudes of external perturbations are $\delta f_1 = 0.02F$ and $\delta f_2 = 0.05F$.

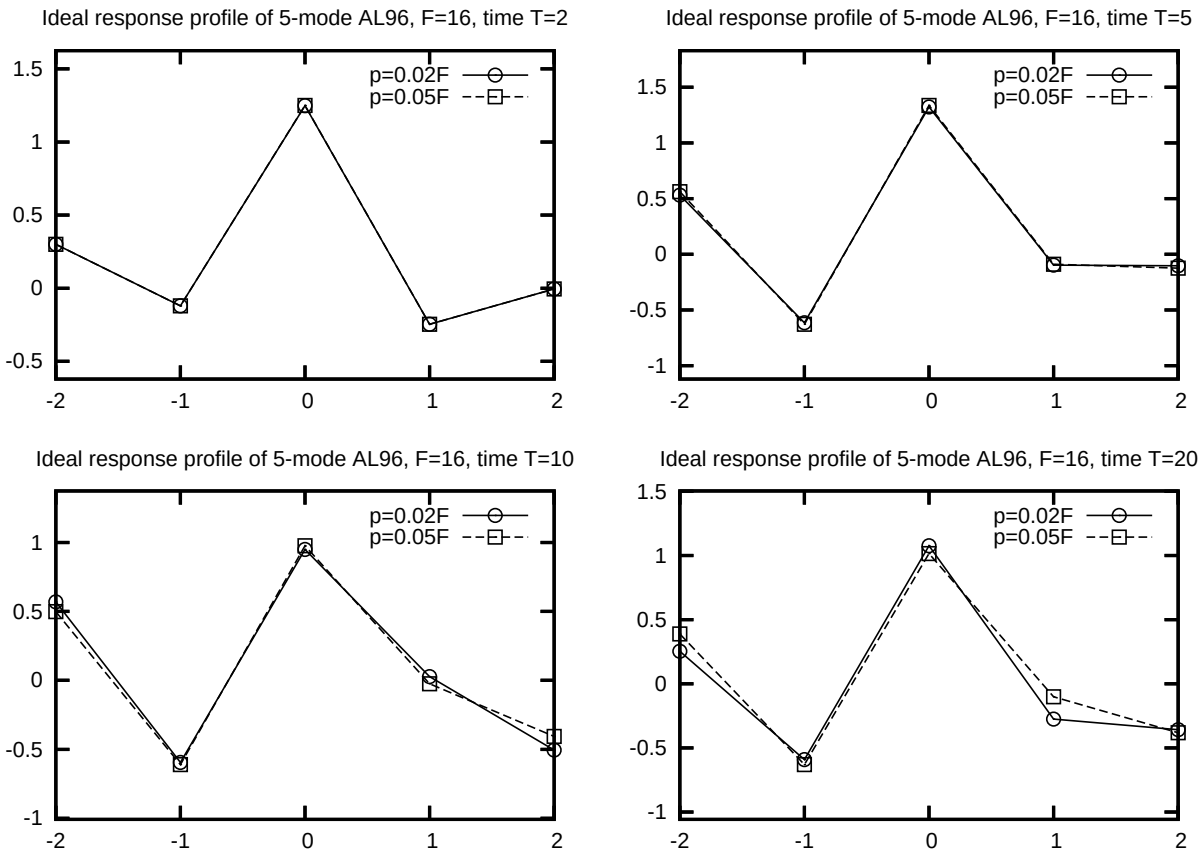

Figure 4.10: Snapshots of the ideal response operators at time $T = 2, 5, 10, 20$ for the 5-mode AL96 model, $F = 16$. Magnitudes of external perturbations are $\delta f_1 = 0.02F$ and $\delta f_2 = 0.05F$.

5 Summary

In the present work we develop and test two new approaches for predicting linear response of a chaotic nonlinear dynamical system with forcing and dissipation to small external perturbation through long-term observations of behavior of the unperturbed model. Both approaches are based on an appropriate version of the fluctuation-dissipation theorem, which is suitable for predicting the response for systems with Sinai-Ruelle-Bowen equilibrium probability measures whose solutions often live on chaotic fractal attractors. The theoretical background and derivation for both methods can be found in Section 2.

The first, more simple, and also more general approach is called the short-time FDT (ST-FDT), and is a direct generalization of the classical fluctuation-dissipation theorem for a dynamical system with arbitrary long-time equilibrium state. The ST-FDT method is tailored to work with a general chaotic dynamical system due to the fact that no prior assumption is made on the equilibrium state of the dynamical system, but has an intrinsic numerical instability because of exponentially growing tangent map of a chaotic dynamical system due to positive Lyapunov exponents. The latter disadvantage limits the ability of the ST-FDT method to predict the response to rather short times, bounded by the reciprocal of the magnitude of the largest Lyapunov exponent.

The second, more sophisticated approach, is called the hybrid Axiom A FDT (hA-FDT). As follows from its name, it is based on the assumption of uniform hyperbolicity of the set of nonwandering points of the flow (which constitutes the essence of Smale's Axiom A), which allows to split the tangent bundle to the flow in the proximity of the attractor uniformly into three subspaces, associated with positive, negative and zero Lyapunov exponents. This splitting allows one to avoid the exponential blow-up of the tangent map along uniformly expanding subspace associated with positive Lyapunov exponents by "integrating by parts" the chunk of the linear response operator corresponding to the expanding subspace, thus eliminating numerical instability [20]. Here, a hybrid Axiom A FDT method is suggested, where the expanding part of the linear response operator is replaced with the classical quasi-Gaussian FDT formula, restricted to the expanding subspace via standard geometric formulas. The hybrid A-FDT approximation retains the original A-FDT approximation [20] on the fractal dissipative directions of the attractor. There are substantial numerical issues in calculating the unstable response formula directly for Axiom A attractors while most geophysical systems of interest are not likely to have Axiom A attractors anyway, so the hybrid A-FDT approximation is a useful one.

Both methods are tested, compared with the classical quasi-Gaussian FDT (qG-FDT) formula and verified against the ideal directly measured response for a simple chaotic AL96 model with 5 degrees of freedom. The AL96 model is essentially the modified Lorenz 96 model with forcing and dissipation where the nonlinear part of the model assumes opposite sign. Despite its simplicity and low dimension, it is demonstrated in Section 3 that the AL96 model has remarkable mixing properties even in weakly and moderately chaotic regimes, which makes it an ideal toy model for testing new FDT methods. Oddly, the 5-mode original Lorenz 96 model (L96) does not exhibit such robust mixing properties for the same range of dynamical regimes, while being slightly more chaotic than the AL96 model, which is also

documented in Section 3.

The results of systematic testing of the ST-FDT, hA-FDT and qG-FDT methods for the 5-mode AL96 model are shown in Section 4. Two simple vector-valued response functions were chosen for testing: the linear function $\vec{A}(\vec{x}) = \vec{x}$ and $A_i(\vec{x}) = x_i^2$, which represent responses of climatological mean state and variance, respectively. Also, while $\vec{A}(\vec{x}) = \vec{x}$ is a linear function, $A_i(\vec{x}) = x_i^2$ is nonlinear, which can make a substantial difference for response errors, as explained at the end of Chapter 2 of [16]. All FDT methods are tested for four dynamical regimes of the AL96 model with different degree of chaos: weakly chaotic $F = 6$, moderately chaotic $F = 8$, and two strongly chaotic regimes $F = 12, 16$. The following trends were observed in the behavior of the ST-FDT, hA-FDT and qG-FDT methods:

- **ST-FDT method.** For short times, the ST-FDT response formula is vastly superior to either the qG-FDT or the hA-FDT responses, for both the linear response function $\vec{A}(\vec{x}) = \vec{x}$ and the nonlinear response function $A_i(\vec{x}) = x_i^2$. The reason for such behavior is that the short-time FDT method is a generalization of both the classical qG-FDT and hA-FDT, which does not imply anything about the structure of the equilibrium state beyond irreducibility, and thus is expected to work for a huge variety of dynamical systems, while qG-FDT and hA-FDT involve various approximations. However, the inherent numerical instability of ST-FDT manifests itself at later times, which is clearly observed in Section 4 when for later times the errors of ST-FDT are several orders of magnitude larger than those for hA-FDT and qG-FDT.

- **hA-FDT method.** The hybrid A-FDT formula is clearly superior to the qG-FDT formula for longer times in all dynamical regimes $F = 6, 8, 12, 16$ for the linear response function $\vec{A}(\vec{x}) = \vec{x}$ and the dynamical regimes $F = 6, 8$ for the quadratic response function $A_i(\vec{x}) = x_i^2$. Moreover, for less chaotic dynamical regimes $F = 6, 8$ the hA-FDT method is vastly superior to the qG-FDT method for longer times. This can be attributed to the fact that for less chaotic regimes the response from the stable directions becomes more important, and thus the hA-FDT, correctly capturing the response from the stable directions, provides better overall precision than the qG-FDT formula. This is a direct confirmation of the earlier observation in Chapter 2 of [16], where prediction of the qG-FDT deteriorates significantly for a 40-mode Lorenz 96 model as values of the forcing F descend into less chaotic regimes, and it was observed that this failure occurs mainly on linearly stable Fourier modes which have higher chance to align with the uniformly contracting subspace on the attractor.

- **qG-FDT method.** For longer times, the qG-FDT formula is marginally better than the hA-FDT formula only in the most chaotic and mixing dynamical regime $F = 16$. This can be attributed to the fact that for this dynamical regime the contribution from contracting directions of the tangent bundle is negligible compared with the expanding directions, and the fact that the qG-FDT formula does not capture the response from the stable directions does not affect the results too much. Also, the fact that hA-FDT is inferior to qG-FDT for the regime $F = 16$ despite using the same classical FDT formula for the expanding subspace part of the response, suggests that the 5-mode

AL96 system does not satisfy the Axiom A, and thus the dimension and span of the expanding subspace are not captured correctly everywhere on the attractor.

Generally, it appears that each FDT method studied here tends to occupy its own "niche" where it performs better than its siblings for various reasons. While the ST-FDT method, being the most general of the three, performs significantly better for short times, the strong side of the hA-FDT method is predicting the response for longer times in weakly and moderately chaotic regimes, where neither ST-FDT nor qG-FDT methods work well. The qG-FDT method, despite its simplicity, holds its own in strongly chaotic regimes for longer times. Future research in this direction will be centered at testing the three methods for more sophisticated models with large-scale features of the real atmosphere and climate, like the 40-mode Lorenz 96 model, and more realistic T21 truncation of the barotropic quasi-geostrophic equations on the sphere with realistic orography and forcing. Also, given the outstanding performance of the hA-FDT for weakly and moderately chaotic regimes for longer times, it is interesting to develop a robust numerical method to compute the true Axiom A response directly through calculating spatial derivatives of the tangent map as outlined in Section 2. Should such a method be developed in the future, it would be extremely important to study its behavior for similar environment.

Acknowledgment. Rafail Abramov is supported by the NSF grant DMS-0608984 and the ONR grant N00014-06-1-0286. Andrew Majda is partially supported by the NSF grant DMS-0456713 and the ONR grant N00014-05-1-0164.

A Numerical algorithm for the tangent map

The evolution equation for the tangent map $T^t_{\vec{x}}$ from (2.23) is

$$\frac{\mathrm{d}}{\mathrm{d}t}T^t_{\vec{x}_0} = \nabla\vec{f}(\vec{x}(t))T^t_{\vec{x}_0} \quad \text{with} \quad T^0_{\vec{x}_0} = I, \tag{A.1}$$

which requires parallel computation of (2.1) together with (A.1). Solving (A.1) directly leads to the same issue with exponential growing of $T^t_{\vec{x}}$, as was mentioned earlier in Section 2. However, there is a way to compute the tangent map $T^t_{\vec{x}}$ as a product of a sequence of orthogonal and upper-triangular matrices, where the norm of each of those matrices by itself is sufficiently small so that the method for computing them is numerically stable.

The suggested numerical method to compute (A.1) is described in [5]. The key idea behind this method is based upon the fact that, due to the special form of (A.1), if a solution of (A.1) is multiplied by a constant, the result is also a valid solution for (A.1) (although with different initial condition). Let Δt be the time step of a numerical discretization for (A.1). Now, at each step of numerical integration of (A.1), we perform a QR-decomposition of $T^t_{\vec{x}}$

$$T^{\Delta t}_{\vec{x}(i\Delta t)} = Q_i R_i, \tag{A.2}$$

where Q_i is the orthogonal matrix and R_i is the upper-triangular matrix with nonnegative diagonal entries. Then, $T^{i\Delta t}$ is replaced with Q_i in (A.1) at each step of numerical integration, which effectively eliminates exponential growth of the solution for (A.1), since columns of Q_i are always unit vectors. Now, starting at m time steps, after n time steps the tangent map $T^{n\Delta t}_{\vec{x}(m\Delta t)}$ can be reconstructed as

$$T^{n\Delta t}_{\vec{x}(m\Delta t)} = Q_{m+n} R_{m+n} \dots R_{m+1} Q_m^T. \tag{A.3}$$

The formula in (A.3) helps to avoid computing (A.1) separately for each point $\vec{x}(t)$ on the trajectory, allowing to have only one instance of the numerical implementation for (A.1) running at any time. Apparently, $Q_0 = I$, since it is the initial condition at time zero. The set of upper-triangular matrices $R_{m+n}, \dots, R_{m+1}$ stores the magnitudes of growth and decay of Lyapunov directions of $T^t_{\vec{x}}$ from the time step m till the time step $m+n$, whereas the orthogonal matrices Q_m, Q_n store the rotation (or twisting) of those directions.

B Numerical algorithm for projection operators

In this section we describe how to compute the expanding, neutral and contracting projection operators P^+, P^0 and P^-. The technical difficulty here is that the subspaces E^+, $E^0 = \vec{f}$ and E^- are typically far from being orthogonal in the Euclidean metric, and thus it is not possible to compute operator P^+ separately from either P^0 or P^-.

Before we proceed further, let us introduce a suitable set of notations regarding spanning sets of E^+, E^0 and E^-:

1. Let N^+ and N^- denote the dimension of expanding subspace E^+ and E^-, respectively, with an obvious relation $N^+ + N^- + 1 = N$, where N is the total dimension of the phase space.
2. Let $\vec{e}^+_k(x)$, $1 \le k \le N^+$ denote the k-th unit vector (with respect to the Euclidean norm) spanning E^+ at x.
3. Let $\vec{e}^-_k(x)$, $1 \le k \le N^-$ denote the k-th unit vector spanning E^- at x.
4. Let $\vec{e}^0(x) = \vec{f}(\vec{x})/\|\vec{f}(\vec{x})\|$ denote the unit vector in the direction of the flow at $\vec{x}$.

Below we outline the numerical algorithm to compute $\vec{e}^+_k(x)$, $\vec{e}^-_k(x)$, and also compute explicit formulas for projection operators $P^+_{\vec{x}}$, $P^-_{\vec{x}}$ and $P^0_{\vec{x}}$.

B.1 Computation of expanding spanning vectors

The evolution equation for a spanning vector e^+_k along the trajectory $x(t)$ happens to be the same as the one for the tangent map in (A.1). Since at a discretization time step i the solution of (A.1) is given by the orthogonal matrix Q_i from (A.2), the first N^+ columns of Q_i are automatically the orthogonal spanning vectors $\vec{e}^+_k$. This algorithm also happens to be extremely tolerant to numerical errors, since projections of $\vec{e}^+_k$ onto E^- (which are errors) decay exponentially fast.

B.2 Computation of contracting spanning vectors

We compute a numerical approximation for $\vec{e}_k^{\leftarrow}$ using the method suggested in [5]. Denoting by D_i the result of setting all off-diagonal entries in R_i from (A.2) to zero, we consider the following matrix:

$$E_n = \left[D_{m+1}^{-1}(\ldots(D_{m+n-1}^{-1}(D_{m+n}^{-1}R_{m+n})R_{m+n-1})\ldots)R_{m+1}\right]^{-1} \tag{B.1}$$

(the placement of brackets defines the ordering for the matrix multiplication to avoid numerical instability). Following Eckmann and Ruelle [5], in the limit as $n \to \infty$, the last column of E_n spans the fastest decaying Lyapunov subspace at the time step m, the last two columns span the second fastest decaying Lyapunov subspace, and so forth. Thus, if the dimension of E^- is N^-, then the last N^- columns of E_n span E^- at the time step m in the limit as $n \to \infty$. Although these columns are not orthogonal, there is an easy method to construct an orthogonal basis for E^- from E_n using QR-decomposition.

Let $\tilde{E}_n$ denote the matrix which is a result of column rearrangement of E_n from (B.1) in reverse order, such that the first column of E_n is the last in $\tilde{E}_n$, the second column of E_n is the second-to-last in $\tilde{E}_n$, and so forth. Then we perform the QR-decomposition on $\tilde{E}_n$:

$$\tilde{E}_n = Q_E R_E. \tag{B.2}$$

Now first N^- columns of $Q_m Q_E$ are the orthogonal vectors $\vec{e}_k^{\leftarrow}$ for the contracting subspace E^- at the time step m. In practice it is not possible to set n in (B.2) to ∞, however for finite n the approximate basis should be good for at least the time scale of $n\Delta t$, which allows to control the precision by choosing sufficiently large n.

B.3 Explicit formulas for projection operators

As we mentioned before, subspaces E^+, E^- and unit vector $\vec{e}^0$ are not orthogonal in general. In order to compute the projection of an arbitrary small forcing $\delta\vec{f}$ onto any spanning vector correctly, we have to know all spanning vectors $\vec{e}_k^{\rightarrow}$ and $\vec{e}_k^{\leftarrow}$ for E^+ and E^-, respectively (which are computed via the algorithms above), and also vector $\vec{e}^0$. In order to write all the formulas in a more efficient manner, we will introduce N vectors $\vec{a}_k$, $1 \le k \le N$, such that

1. $\vec{a}_k = \vec{e}_k^{\rightarrow}(x)$ for $1 \le k \le N^+$,
2. $\vec{a}_{k+N^+} = \vec{e}_k^{\leftarrow}(x)$ for $1 \le k \le N^-$,
3. $\vec{a}_N = \vec{e}^0(x)$,
4. Let A_{kj} denote the matrix whose columns are $\vec{a}_k$, $1 \le k \le N$.

The reason we introduce the notation $\vec{a}_k$ is that it allows to integrate together the notations for $\vec{e}_k^{\rightarrow}$, $\vec{e}_k^{\leftarrow}$ and $\vec{e}^0$, and to produce the matrix A_{kj} whose columns 1 through N^+ are $\vec{e}_k^{\rightarrow}$, columns $N^+ + 1$ through $N^+ + N^-$ are $\vec{e}_k^{\leftarrow}$, and the last column is $\vec{e}^0$.

Let $\vec{v} \in \mathbb{R}^N$ be an arbitrary vector, and let c_k be the set of expansion coefficients of $\vec{v}$ with respect to $\vec{a}_k$:

$$\vec{v} = \sum_{k=1}^{N} c_k \vec{a}_k, \tag{B.3}$$

or, in matrix-vector notation,

$$A\vec{c} = \vec{v}. \tag{B.4}$$

The latter yields

$$\vec{c} = A^{-1}\vec{v}. \tag{B.5}$$

Thus, the projection operator P_k onto $\vec{a}_k$ is

$$P_k = \vec{a}_k \otimes \vec{A}_k^{-1}, \tag{B.6}$$

where $\vec{A}_k^{-1}$ denotes the k-th row of A^{-1}. The operators P^+, P^- and P^0 are then

$$P^+ = \sum_{k=1}^{N^+} P_k, \qquad P^- = \sum_{k=N^++1}^{N^++N^-} P_k, \qquad P^0 = P_N. \tag{B.7}$$

References

[1] R. Abramov and A. Majda. Quantifying uncertainty for non-Gaussian ensembles in complex systems. *SIAM J. Sci. Comp.*, 26(2):411–447, 2003.

[2] T. Bell. Climate sensitivity from fluctuation dissipation: Some simple model tests. *J. Atmos. Sci.*, 37(8):1700–1708, 1980.

[3] G. Carnevale, M. Falcioni, S. Isola, R. Purini, and A. Vulpiani. Fluctuation-response in systems with chaotic behavior. *Phys. Fluids A*, 3(9):2247–2254, 1991.

[4] B. Cohen and G. Craig. The response time of a convective cloud ensemble to a change in forcing. *Quart. J. Roy. Met. Soc.*, 130(598):933–944, 2004.

[5] J. Eckmann and D. Ruelle. Ergodic theory of chaos and strange attractors. *Rev. Mod. Phys.*, 57(3):617–656, 1985.

[6] D. Evans and G. Morriss. *Statistical Mechanics of Nonequilibrium Liquids.* Academic Press, New York, 1990.

[7] A. Gritsoun. Fluctuation-dissipation theorem on attractors of atmospheric models. *Russ. J. Numer. Math. Modeling*, 16(2):115–133, 2001.

[8] A. Gritsoun and G. Branstator. Climate response using a three-dimensional operator based on the fluctuation-dissipation theorem. *J. Atmos. Sci.*, 2007. Accepted for publication.

[9] A. Gritsoun, G. Branstator, and V. Dymnikov. Construction of the linear response operator of an atmospheric general circulation model to small external forcing. *Num. Anal. Math. Modeling*, 17:399–416, 2002.

[10] A. Gritsoun and V. Dymnikov. Barotropic atmosphere response to small external actions. theory and numerical experiments. *Atmos. Ocean Phys.*, 35(5):511–525, 1999.

[11] K. Haven, A. Majda, and R. Abramov. Quantifying predictability through information theory: Small sample estimation in a non-Gaussian framework. *J. Comp. Phys.*, 206:334–362, 2005.

[12] R. Kubo, M. Toda, and N. Hashitsume. *Statistical Physics II: Nonequilibrium Statistical Mechanics*. Springer-Verlag, New York, 1985.

[13] C. Leith. Climate response and fluctuation-dissipation. *J. Atmos. Sci.*, 32:2022–2025, 1975.

[14] E. Lorenz. Predictability: A problem partly solved. In *Proceedings of the Seminar on Predictability*, Shinfield Park, Reading, England, 1996. ECMWF.

[15] E. Lorenz and K. Emanuel. Optimal sites for supplementary weather observations. *J. Atmos. Sci.*, 55:399–414, 1998.

[16] A. Majda, R. Abramov, and M. Grote. *Information Theory and Stochastics for Multiscale Nonlinear Systems*, volume 25 of *CRM Monograph Series of Centre de Recherches Mathématiques, Université de Montréal*. American Mathematical Society, 2005. ISBN 0-8218-3843-1.

[17] S. Orszag and J. McLaughlin. Evidence that random behavior is generic for nonlinear differential equations. *Physica D*, 1:68–79, 1980.

[18] F. Risken. *The Fokker-Planck Equation*. Springer-Verlag, New York, second edition, 1988.

[19] D. Ruelle. Differentiation of SRB states. *Comm. Math. Phys.*, 187:227–241, 1997.

[20] D. Ruelle. General linear response formula in statistical mechanics, and the fluctuation-dissipation theorem far from equilibrium. *Phys. Lett. A*, 245:220–224, 1998.

[21] L.-S. Young. What are SRB measures, and which dynamical systems have them? *J. Stat. Phys.*, 108(5-6):733–754, 2002.